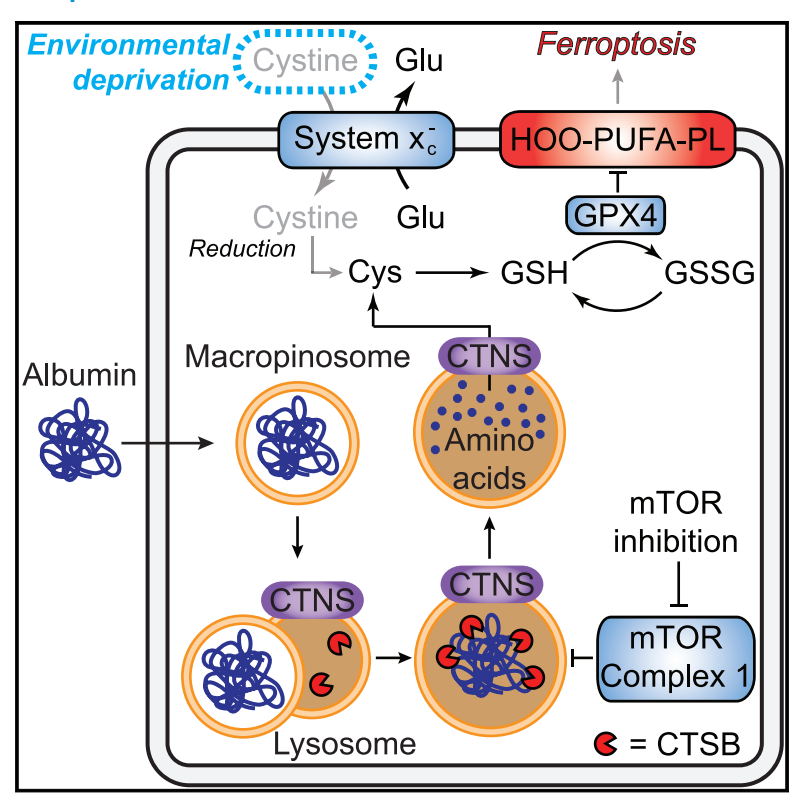
# Ferroptosis inhibition by lysosome-dependent catabolism of extracellular protein

#### **Graphical abstract**



#### **Authors**

David A. Armenta, Nouf N. Laqtom, Grace Alchemy, ..., David A. Nathanson, Monther Abu-Remaileh, Scott J. Dixon

#### Correspondence

monther@stanford.edu (M.A.-R.), sjdixon@stanford.edu (S.J.D.)

#### In brief

Mechanisms that regulate ferroptosis sensitivity and resistance remain poorly defined. Armenta et al. demonstrate that uptake and lysosomal catabolism of extracellular protein can prevent ferroptosis in cystine-deprived cells by maintaining intracellular levels of cysteine and glutathione. This compensatory mechanism may limit the effectiveness of cancer therapies that target cystine uptake.

#### **Highlights**

- Extracellular albumin can block ferroptosis caused by cystine deprivation
- Albumin is cysteine rich and, when catabolized, can replenish GSH stores
- Lysosomal albumin catabolism requires cathepsin B (CTSB)
- Extracellular albumin suppresses ferroptosis in spheroid cell models







#### **Article**

# Ferroptosis inhibition by lysosome-dependent catabolism of extracellular protein

David A. Armenta, <sup>1,6</sup> Nouf N. Laqtom, <sup>2,3,4,6</sup> Grace Alchemy, <sup>1</sup> Wentao Dong, <sup>2,3,4</sup> Danielle Morrow, <sup>5</sup> Carson D. Poltorack, <sup>1</sup> David A. Nathanson, <sup>5</sup> Monther Abu-Remaileh, <sup>2,3,4,\*</sup> and Scott J. Dixon<sup>1,7,\*</sup>

- <sup>1</sup>Department of Biology, Stanford University, Stanford, CA 94305, USA
- <sup>2</sup>Department of Chemical Engineering, Stanford University, Stanford, CA 94305, USA
- <sup>3</sup>Department of Genetics, Stanford University, Stanford, CA 94305, USA
- <sup>4</sup>The Institute for Chemistry, Engineering, & Medicine for Human Health (ChEM-H), Stanford University, Stanford, CA 94305, USA
- <sup>5</sup>Department of Molecular & Medical Pharmacology, University of California, Los Angeles, Los Angeles, CA 90095, USA
- <sup>6</sup>These authors contributed equally
- 7Lead contact
- \*Correspondence: monther@stanford.edu (M.A.-R.), sjdixon@stanford.edu (S.J.D.) https://doi.org/10.1016/j.chembiol.2022.10.006

#### **SUMMARY**

Cancer cells need a steady supply of nutrients to evade cell death and proliferate. Depriving cancer cells of the amino acid cystine can trigger the non-apoptotic cell death process of ferroptosis. Here, we report that cancer cells can evade cystine deprivation-induced ferroptosis by uptake and catabolism of the cysteine-rich extracellular protein albumin. This protective mechanism is enhanced by mTORC1 inhibition and involves albumin degradation in the lysosome, predominantly by cathepsin B (CTSB). CTSB-dependent albumin breakdown followed by export of cystine from the lysosome via the transporter cystinosin fuels the synthesis of glutathione, which suppresses lethal lipid peroxidation. When cancer cells are grown under non-adherent conditions as spheroids, mTORC1 pathway activity is reduced, and albumin supplementation alone affords considerable protection against ferroptosis. These results identify the catabolism of extracellular protein within the lysosome as a mechanism that can inhibit ferroptosis in cancer cells.

#### INTRODUCTION

For many cancer cells, the thiol-containing amino acid cysteine is conditionally essential for survival and proliferation (Combs and DeNicola, 2019; Eagle, 1959). Cysteine is a proteogenic amino acid but also needed for synthesis of glutathione (GSH), coenzyme A, and other important sulfur-containing metabolites. Among other functions, GSH and coenzyme A are needed to prevent ferroptosis, a non-apoptotic, oxidative form of cell death (Badgley et al., 2020; Dixon et al., 2012; Leu et al., 2019). The function of coenzyme A in ferroptosis is unclear. In contrast, GSH is a co-substrate for glutathione peroxidase 4 (GPX4), an essential enzyme that prevents ferroptosis by reducing potentially toxic membrane lipid hydroperoxides to non-toxic lipid alcohols (Friedmann Angeli et al., 2014; Ingold et al., 2018). The ferroptosis mechanism is an emerging target for anti-cancer therapy (Bartolacci et al., 2022; Hangauer et al., 2017; Jiang et al., 2021; Koppula et al., 2022; Viswanathan et al., 2017). It is therefore of interest to understand how cancer cells manage cysteine metabolism to inhibit ferroptosis.

Cysteine is typically present at low abundance in the cell and in the fluid surrounding tumors *in vivo* (Abu-Remaileh et al., 2017; Sullivan et al., 2019). Depriving cells of extracellular cystine, the disulfide of cysteine typically present outside of the cell,

potently induces ferroptosis in numerous cultured cancer cell lines (Dixon et al., 2014; Poltorack and Dixon, 2021; Yang et al., 2014). Cells can be starved of cystine by small molecules, like erastin, that inhibit the system  $x_c^-$  cystine/glutamate antiporter; by removing cystine from the growth medium of cultured cells; or by degrading extracellular cystine/cysteine using the engineered enzyme cyst(e)inase (Badgley et al., 2020; Cramer et al., 2017; Dixon et al., 2014; Tarangelo et al., 2018; Wang et al., 2019; Zhang et al., 2019). The mechanisms employed by cancer cells to maintain intracellular cysteine levels and prevent onset of ferroptosis under conditions of extracellular cystine limitation are not fully understood.

Protein uptake from the extracellular environment via macropinocytosis or other endosomal processes can fuel cancer cell proliferation and resistance to anti-cancer therapies (Davidson et al., 2017; Jayashankar and Edinger, 2020; Kamphorst et al., 2015; Kim et al., 2018). The abundant serum protein albumin in particular can serve as a source of amino acids to support tumor growth (Commisso et al., 2013; Kamphorst et al., 2015). Catabolism of intracellular or extracellular protein in the lysosome liberates amino acids that can then be exported into the cytosol and used for synthesis of proteins and other products (Cantin et al., 2000; Jayashankar and Edinger, 2020; Kim et al., 2018; Nofal et al., 2021; Palm, 2019; Perera et al., 2015; Wyant



#### **Article**



et al., 2017; Zhang and Commisso, 2019). Whether catabolism of extracellular protein liberates sufficient cysteine to suppress ferroptosis and enable proliferation under cystine-poor conditions is unclear.

Protein catabolism in the lysosome is promoted by inhibition of the mechanistic target of rapamycin complex 1 (mTORC1) (Nofal et al., 2017; Palm et al., 2015; Ratto et al., 2022). We recently showed that mTORC1 inhibition prevents depletion of intracellular GSH and attenuated ferroptosis in cultured cells deprived of cystine (Conlon et al., 2021). In the present study, we tested the hypothesis that mTORC1 inhibition, together with uptake and catabolism of extracellular protein, would be sufficient to compensate for the loss of transporter-mediated cystine uptake and inhibit ferroptosis. We find that uptake and lysosomal catabolism of extracellular albumin, a cysteine-rich protein, is sufficient to prevent cancer cells deprived of extracellular free cystine from undergoing ferroptosis. This protective mechanism requires the lysosomal enzyme cathepsin B and the lysosomal cystine exporter cystinosin. This mechanism enables extracellular albumin to fuel ongoing GSH synthesis in the cell in the absence of cystine uptake from the environment.

#### **RESULTS**

# Cystine deprivation triggers ferroptosis, which can be suppressed by extracellular albumin

How cancer cells cope with limited extracellular amino acids, especially cystine, is not entirely clear. To investigate this, we deprived HT-1080<sup>N</sup> fibrosarcoma cells of cystine and measured cell proliferation and cell death over time. These cells express a live cell marker, nuclear-localized mKate2 (denoted by the superscript "N") and were incubated with the dead cell dye SYTOX Green. This enabled cell proliferation and cell death to be directly quantified using the scalable time-lapse analysis of cell death kinetics (STACK) method (Forcina et al., 2017; Inde et al., 2021). Cells cultured in complete medium proliferated rapidly for 4 days and then died. This was most likely due to overcrowding-induced apoptosis (Forcina et al., 2017), because this death was blocked by the pan-caspase inhibitor Q-VD-OPh (Figures 1A and 1B). In contrast, cells selectively deprived of cystine by culture in cystine-free medium did not proliferate and mostly died within 24 h in a manner that was suppressed by the ferroptosis-specific inhibitor ferrostatin-1 (Fer-1) but not by Q-VD-OPh (Figures 1A and 1B). Selective deprivation of three other amino acids (Met, Arg, and Leu) from the culture medium resulted in proliferative arrest and/or a minimal amount of cell death over 8 days that was not affected by Fer-1 (Figures 1A and 1B). Thus, cultured HT-1080 cells are specifically sensitive to induction of ferroptosis upon deprivation of extracellular

Cystine deprivation *in vivo* can slow tumor growth but does not appear to cause consistent tumor regression (Badgley et al., 2020; Wang et al., 2019; Zhang et al., 2019). This suggests that compensatory mechanisms may exist that limit ferroptosis in response to cystine deprivation. In addition to transporter-mediated uptake of free amino acids, cancer cells can internalize and catabolize extracellular protein, which can contain extensive endogenous and bound cysteine (Eagle et al., 1960; Palm, 2019; Zhang and Commisso, 2019). The catabolism of ingested

protein can be increased by mTOR inhibition (Nofal et al., 2017; Palm et al., 2015). We recently found that mTORC1 inhibition inhibits ferroptosis in response to cystine deprivation (Conlon et al., 2021). Accordingly, we hypothesized that providing cells with additional extracellular cysteine-containing protein, together with mTORC1 inhibition, would be sufficient to prevent ferroptosis in cells deprived of free extracellular cystine. As an extracellular protein source, we first tested the abundant serum protein albumin at a final concentration (3% [w/v]) mimicking that found in human serum (Choi et al., 2004; Keyser et al., 1981). Consistent with our recent results (Conlon et al., 2021), treatment with the ATP-competitive mTOR inhibitor INK128 alone was sufficient to attenuate cystine deprivation-induced cell death, albeit to a limited extent, over 7 days (Figures 1C and 1D). Incubating cells in albumin-enriched medium alone likewise partially inhibited cell death over time in response to cystine deprivation (Figures 1C and 1D). In contrast, the combination of albumin and mTOR inhibitor (A+I) potently suppressed cell death under cystine-deprived conditions for at least 7 days (Figures 1C and 1D). In addition to HT-1080<sup>N</sup> cells, A+I treatment suppressed cell death in cystine-deprived H1299<sup>N</sup> and H23<sup>Cas9,N</sup> non-small cell lung carcinoma cells and U-2 OSN osteosarcoma, A375N melanoma, T98GN glioblastoma, and PaTu 8988T pancreatic adenocarcinoma cell lines, consistent with a broadly generalizable effect (Figures 1E and S1A).

We investigated the nature of the A+I protective effect. The ability of A+I treatment to inhibit ferroptosis in cells deprived of cystine was concentration dependent for albumin and INK128, indicating a titratable effect (Figures S1B and S1C). This protective effect was also observed when using structurally distinct mTOR inhibitors (Torin 1 and rapamycin) in combination with albumin, suggesting that the protective mechanism was not linked to INK128 per se (Figures S1D and S1E). The mTOR kinase is present in two distinct signaling complexes, mTORC1 and mTORC2. Short hairpin RNA (shRNA) targeting the mTORC1 subunit RPTOR, but not the mTORC2 complex subunit RICTOR. could substitute for pharmacological mTOR inhibition in protecting cells from cystine deprivation-induced death when combined with extracellular albumin (Figures S1F and S1G). These results argued that our pharmacological mTOR inhibitor treatments were acting in an on-target manner and that mTORC1 inhibition was required for albumin to protect against ferroptosis.

We considered potential alternative explanations for the ability of A+I to inhibit ferroptosis in response to cystine deprivation beyond effects on cysteine metabolism, including general suppression of cell death, induction of cell cycle arrest or autophagy (i.e., by mTORC1 inhibition), and altered iron homeostasis. A+I treatment did not appear to be a general suppressor of cell death as this treatment prevented cell death in response to the small molecule system  $x_c^-$  inhibitor erastin2, which blocks cystine uptake (Dixon et al., 2014), but not in response to small-molecule inhibitors of the proteasome, topoisomerase function, microtubule integrity, or other essential functions (Figure 1F). The protective effect of the A+I combination was not recapitulated in HT-1080 cells by the combination of albumin and the CDK4/ 6 inhibitor palbociclib, suggesting that proliferative arrest was insufficient to explain the protective effects of albumin co-treatment (Figures S2A and S2B). Moreover, A+I treatment protected equally well against ferroptosis in control and ATG7

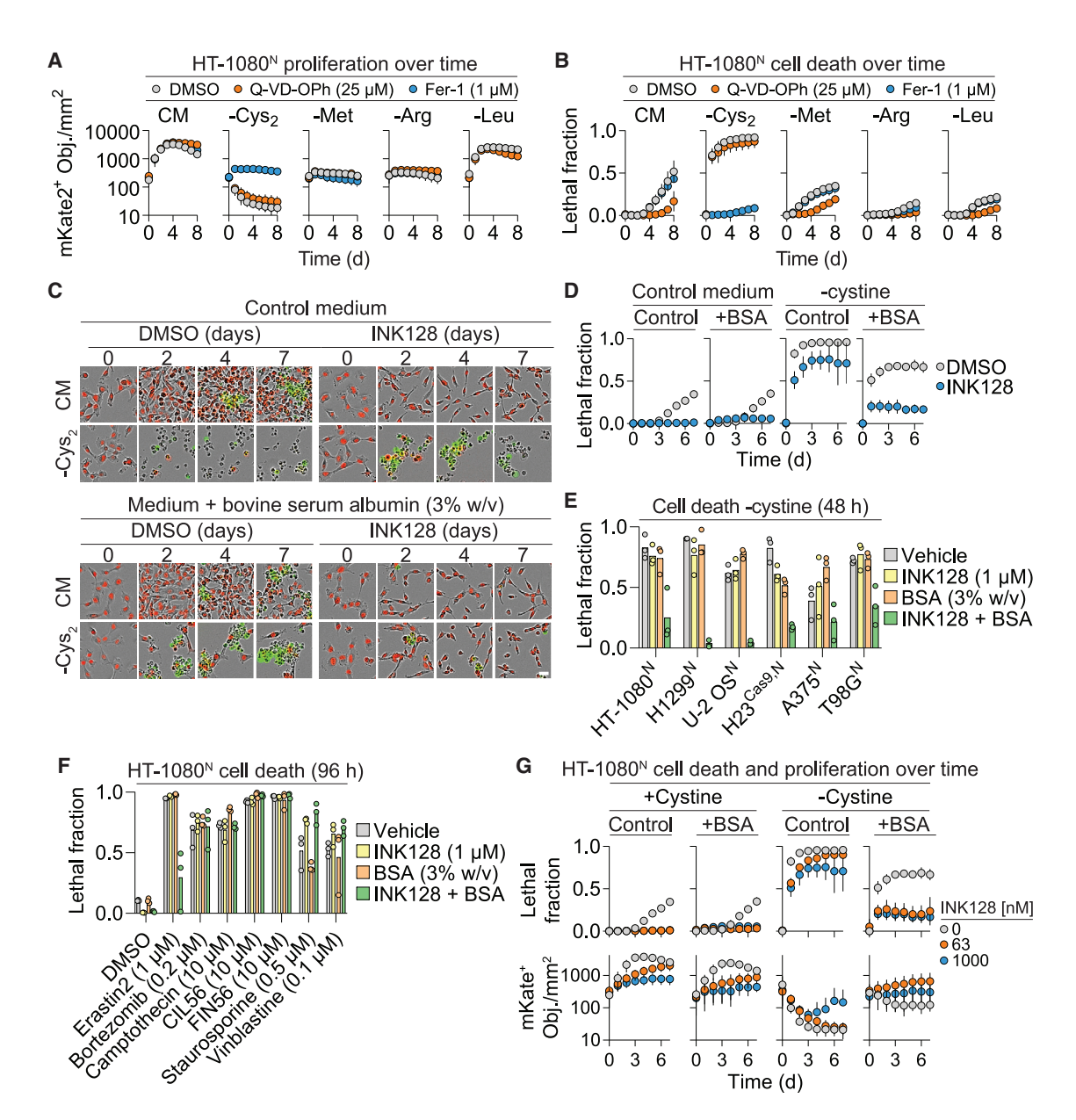


Figure 1. Albumin promotes cell survival in response to cystine deprivation

(A) Cell proliferation determined by live cell (nuclear-mKate2-positive objects [mKate2+ Obj.]) counts over time in complete medium (CM) or medium lacking the indicated amino acid with or without apoptosis (Q-VD-OPh) or ferroptosis (Fer-1) inhibitors. Cys<sub>2</sub>, cystine.

- (B) Cell death in populations from (A), determined by integration of live (mKate2+) and dead (SYTOX Green-positive) counts over time into the lethal fraction score (Forcina et al., 2017). A lethal fraction score of 0 equals no cell death, and 1 equals complete population cell death.
- (C) Representative images from three independent experiments of HT-1080<sup>N</sup> cells cultured over time in CM or medium lacking Cys<sub>2</sub>. Medium contains 20 nM SYTOX Green to mark dead cells. INK128, 1 μM. Scale bar, 30 μm.
- (D) Quantification of cell death in (C). BSA, bovine serum albumin.
- (E) Cell death in different cell lines in medium lacking Cys<sub>2</sub>.
- (F) Cell death in response to different inducers of cell death.
- (G) Cell death and proliferation over time. Some of the lethal fraction data shown here for comparison are also depicted in (D). These data were from the same experiment.

Results in (A), (B), (D), and (G) are mean ± SD from three independent experiments. Data points from independent experiments are shown in (E) and (F). See also Figures S1 and S2.

gene-disrupted (knockout [KO]) PaTu 8988T cell lines, suggesting that autophagy was not likely to be essential for this effect (Figures S2C and S2D). Finally, A+I treatment did not increase

expression of the anti-ferroptotic proteins GPX4 or FSP1 in HT-1080 cells (Bersuker et al., 2019; Doll et al., 2019; Yang et al., 2014) or decrease intracellular iron levels, as assessed

#### **Article**



by expression of the transferrin receptor (TFRC) or IRP2, which are induced by iron starvation (Figure S2E). These results argued against several alternative mechanisms of ferroptosis resistance in A+I-treated cells.

In response to amino acid deprivation, the combination of albumin with low doses of mTOR inhibitor can enable some amount of cell proliferation (Palm et al., 2015). In line with this finding, the combination of albumin with low-dose INK128 (63 nM) not only inhibited ferroptosis but was compatible with some cell proliferation under cystine-free conditions (Figure 1G). These results supported the hypothesis that extracellular protein specifically inhibited ferroptosis and enabled cell proliferation when cystine was not present, through a mechanism that was enhanced by mTORC1 inhibition. These results also further argued against a protective mechanism that involved iron deprivation because this would be expected to arrest cell proliferation.

#### Albumin fuels GSH synthesis to suppress ferroptosis

Ferroptosis is caused by compromised defense against the accumulation of toxic lipid hydroperoxides. Given our results, we hypothesized that A+I treatment would prevent membrane lipid peroxidation in cystine-deprived cells. Consistent with this hypothesis, oxidation of the lipid peroxidation sensor C11 BODIPY 581/591 was strongly suppressed by the A+I combination (Figure 2A). Albumin is reported to act as a direct antioxidant and can also bind other molecules known to inhibit lipid peroxidation, like oleic acid (Carballal et al., 2003; Magtanong et al., 2019; Neuzil et al., 1993), suggesting two additional alternative mechanisms that could explain reduced levels of lipid peroxidation and ferroptosis. Albumin treatment alone weakly inhibited ferroptosis in response to low doses of the GPX4 inhibitors FIN56 and ML162 (Shimada et al., 2016) (Figure S2F). However, this protective effect was lost at high doses of ML162 and FIN56 and, unlike in cystine-deprived cells, not enhanced by mTOR inhibition (Figures 1F, 2B, and S2F). Thus, although albumin may partially inhibit lipid peroxidation and ferroptosis through a direct antioxidant or related effect, the A+I combination strongly suppresses ferroptosis only in response to cystine deprivation.

The results obtained so far bolstered our working model that A+I treatment blocked ferroptosis in response to cystine deprivation by providing an alternate cysteine source. This model was supported by several additional lines of evidence. First, compared with other proteins, albumin is both highly abundant in serum and rich in cysteine residues compared to other proteins (Geyer et al., 2016; Figure S3A). Albumin (35 cysteines/ molecule) was a more potent inhibitor of ferroptosis than the less cysteine-rich molecules ovalbumin (6 cysteines/molecule) or casein (1 cysteine/molecule) when added to cells in the same proportion (Figure 2C). Second, albumin treatment modulated a canonical biochemical marker of amino acid starvation, accumulation of activating transcription factor 4 (ATF4) (Conlon et al., 2021; Wortel et al., 2017); accumulation of ATF4 in response to 10 h of cystine deprivation was inhibited by addition of extracellular albumin (Figure 2D). Cells were harvested at 10 h as waiting longer would mean that cystine-deprived control cells would start to die. It is likely that the partial inhibition of ATF4 accumulation by albumin treatment alone is transient, consistent with the partial suppression of cell death (Figure 1D). mTOR inhibition decreases ATF4 mRNA transcription (Park et al., 2017), reducing the pool of ATF4 mRNA available to translate, likely accounting for the blunting effect of INK128 and combined A+I treatment on ATF4 levels. Some evidence suggests that ATF4 may accumulate in response to oxidative stress (Wortel et al., 2017), which, in the context of ferroptosis, would be downstream of cysteine deprivation per se. However, we found that suppressing lipid peroxide accumulation using Fer-1 did not prevent ATF4 protein from accumulating in response to cystine deprivation or stop albumin from blunting this phenotype, suggesting that ATF4 accumulation was linked to cysteine deprivation and not oxidative stress (Figure S3B). Third, in cells deprived of cystine, A+I treatment largely preserved levels of the downstream cysteine-containing metabolite GSH (Figure 2E). This was functionally important because the ability of A+I to prevent ferroptosis in cystine-deprived HT-1080<sup>N</sup>, A375<sup>N</sup>, H1299<sup>N</sup>, and T98G<sup>N</sup> cancer cell lines was blunted to a variable degree by inhibition of de novo GSH synthesis using buthionine sulfoximine (BSO) (Figures 2F, S3C, and S3D).

These results suggested that extracellular albumin combined with mTOR inhibition could block toxic lipid hydroperoxide accumulation and induction of ferroptosis in response to cystine deprivation by maintaining the intracellular levels of GSH and possibly other sulfur-containing metabolites (Badgley et al., 2020; Leu et al., 2019). We recently showed that stabilization of the transcription factor p53 also leads to conservation of intracellular GSH and ferroptosis inhibition under conditions of cystine deprivation (Tarangelo et al., 2018, 2022). We therefore examined whether p53 stabilization contributed to the protective effects of A+I treatment in response to cystine deprivation. Neither cystine deprivation nor A+I treatment stabilized p53 in HT-1080 or U-2 OS cells (Figure S3E). A+I treatment was also capable of fully suppressing ferroptosis in cystine-deprived H1299 cells, which are p53 deficient (Figures 1E and S3E). Thus, p53 stabilization was not necessary for A+I treatment to protect cells from ferroptosis after cystine deprivation.

#### Lysosomal protease function is required for albumin to suppress ferroptosis

Extracellular albumin is ingested by cancer cells and catabolized within the lysosome to liberate free amino acids, a mechanism that can help cancer cells to survive in nutrient-scarce environments (Commisso et al., 2013; Kamphorst et al., 2015; Nofal et al., 2021; Wyant et al., 2017). We hypothesized that lysosome-dependent proteolytic degradation of ingested albumin liberated free cysteine to stabilize intracellular GSH levels, suppress toxic lipid hydroperoxide accumulation, and inhibit ferroptosis in cystine-deprived cells. We tested this hypothesis by perturbing lysosome activity in different ways. Lysosomal protease activity can be inhibited pharmacologically using deacidifying agents (e.g., chloroquine) or using a cocktail of the protease inhibitors pepstatin A, leupeptin, and E-64 (Palm et al., 2015; Poole and Ohkuma, 1981). Consistent with our hypothesis, co-treatment with chloroquine or the protease inhibitor cocktail prevented A+I treatment from suppressing ferroptosis in cystinedeprived cells (Figure 3A). We confirmed that chloroquine and protease inhibitor cocktail treatment inhibited lysosomal albumin catabolism, as assessed by dequenching of the probe DQ-BSA (Commisso et al., 2013; Reis et al., 1998; Figures 3B, 3C, and

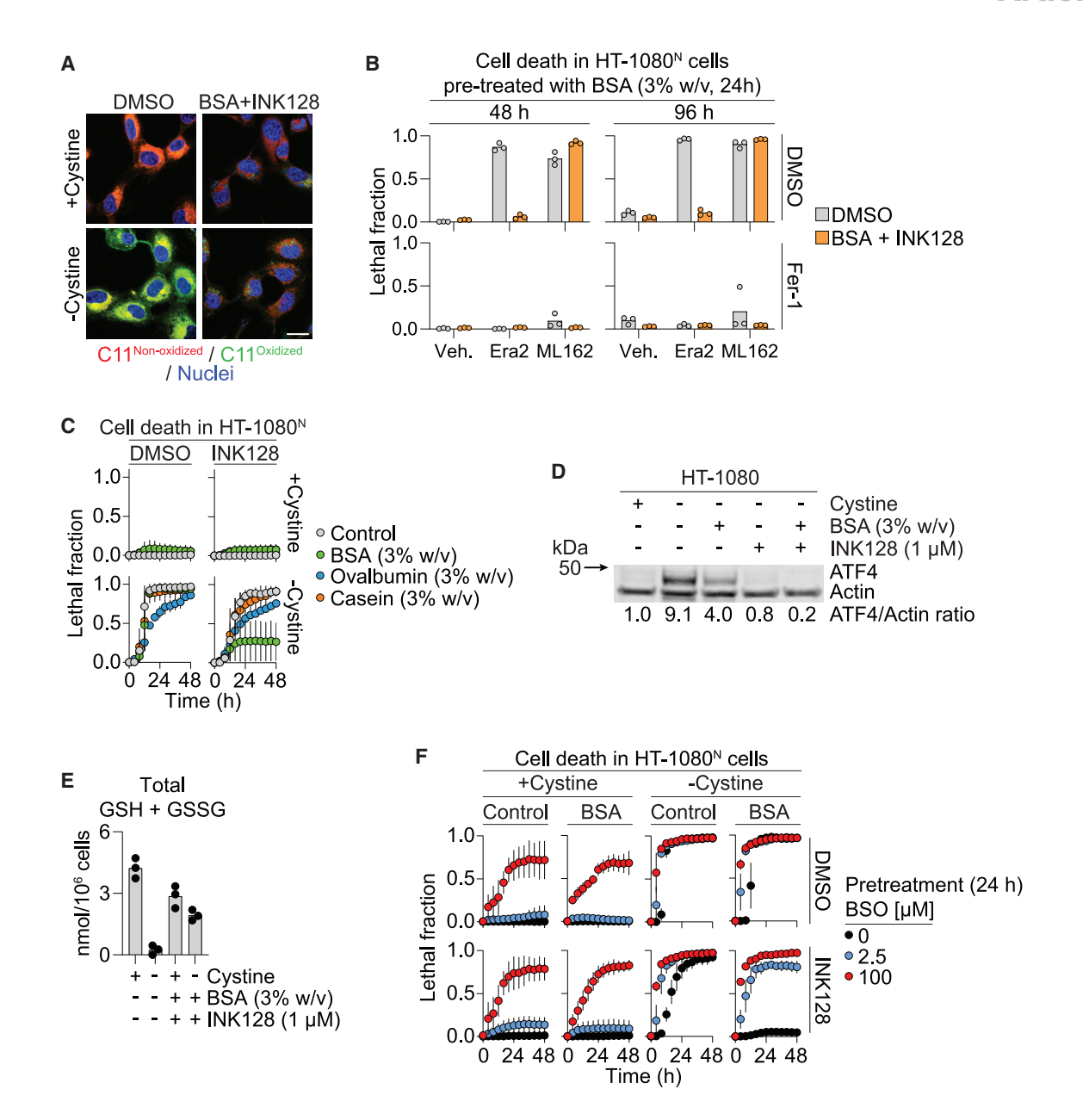


Figure 2. Albumin increases GSH levels during cysteine deprivation

(A) C11 BODIPY 581/591 (C11) oxidation, assessed by confocal microscopy, in HT-1080 cells. BSA, 3% (w/v); INK128,  $1~\mu$ M. Scale bar,  $20~\mu$ m. (B) Cell death in HT-1080<sup>N</sup> cells pre-treated with BSA (24 h) then treated as indicated at time 0 and examined 48 and 96 h later. Era2 (erastin2),  $1~\mu$ M. ML162,  $2~\mu$ M. Fer-1 (ferrostatin-1),  $1~\mu$ M.

- (C) Cell death over time. INK128, 1  $\mu\text{M}.$
- (D) Protein levels after 10 h treatment. The blot is representative of three independent experiments. Mean ATF4/actin protein level ratios (normalized to the +Cys<sub>2</sub> condition), determined from densitometry of three independent blots, are indicated.
- (E) Total GSH (GSH + GSSG) after 8-h treatment. INK128, 1  $\mu$ M.
- (F) Cell death after 24 h pretreatment with or without BSO (buthionine sulfoximine) and then treatment as indicated alongside BSO. BSA, 3% (w/v).

Results in (B) and (E) show datapoints from independent experiments. Results in (C) and (F) are mean ± SD from three independent experiments. See also Figure S3.

S4A). Chloroquine and the protease inhibitor cocktail likewise resulted in accumulation of LC3B, a protein constitutively degraded in the lysosome, although this was more pronounced with chloroquine than with protease inhibitors (Figure S4B). Concordant with these results, ATF4 accumulation, which was blunted in cystine-deprived cells by albumin, INK128, or A+I

treatment, reverted to higher levels upon co-addition of chloroquine or the protease inhibitor cocktail (Figure 3D). Phenotypically, we generalized these results to additional cancer cell lines, showing that chloroquine and/or protease inhibitor cocktail partially reverted the anti-ferroptotic effects of A+I treatment in A375<sup>N</sup>, H1299<sup>N</sup>, and T98G<sup>N</sup> cells (Figures 3E and 3F). The





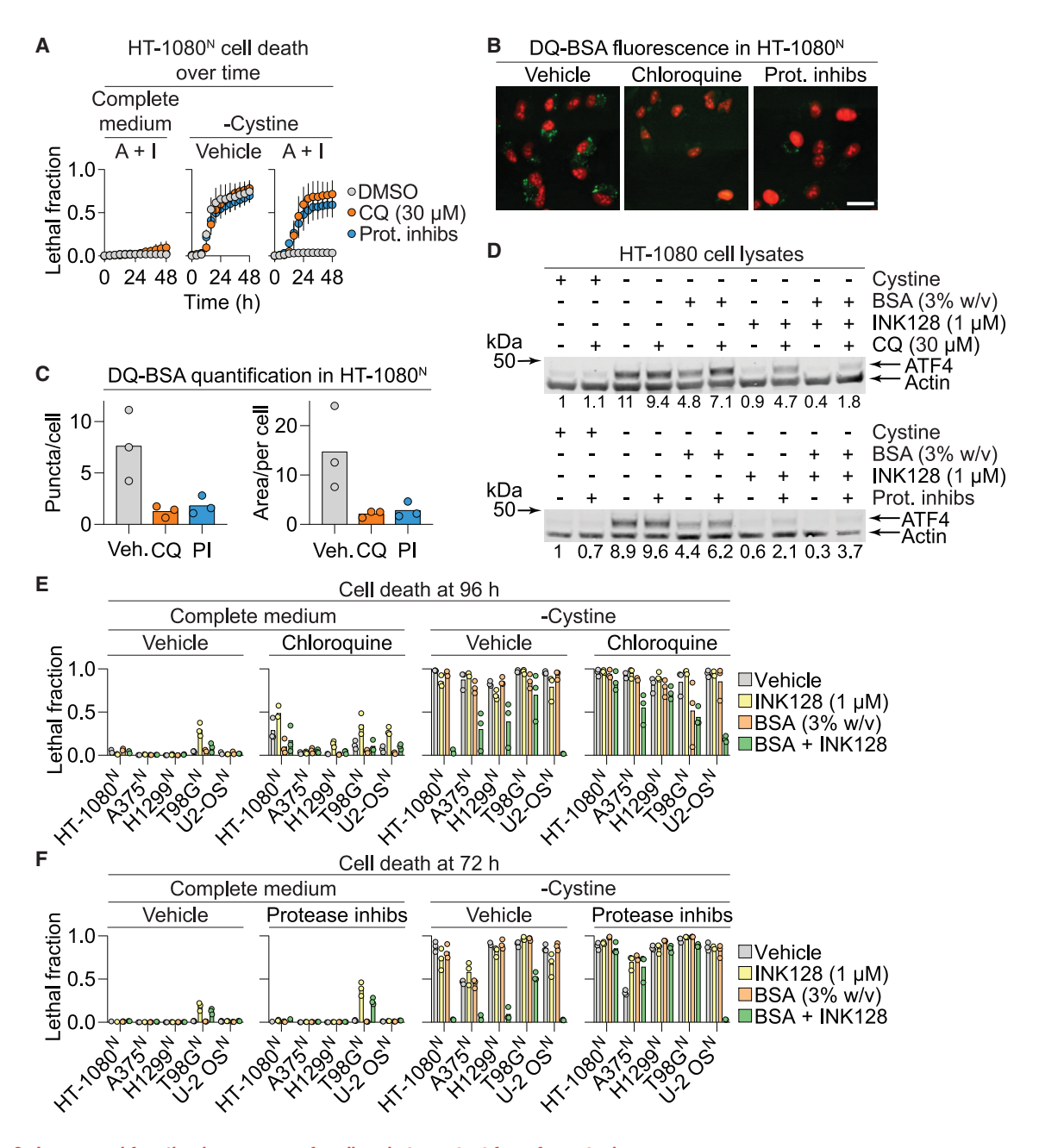


Figure 3. Lysosomal function is necessary for albumin to protect from ferroptosis

(A) Cell death over time. A+I, BSA (3% [w/v]) + INK128 (1 μM). Prot. inhibs, protease inhibitor cocktail (leupeptin, 10 μM; pepstatin A, 2 μM; E-64, 2 μM). Data represent mean ± SD from three independent experiments.

- (B) DQ-BSA fluorescence assessed by fluorescence microscopy in HT-1080<sup>N</sup> cells treated with chloroquine (30 μM) or Prot. inhibs as in (A). Images are representative of three independent experiments. Scale bar, 30 μm.
- (C) Quantification of DQ-BSA puncta or areas (in square pixels) per cell. Datapoints represent counts of puncta from all images within a condition divided by number of cells in those images from three independent experiments (minimum 30 cells/experiment and condition).
- (D) ATF4 protein levels in response to different treatment conditions (10 h). CQ, chloroquine. Blots are representative of three independent experiments. Mean ATF4/Actin protein level ratios (normalized to the +Cys2 condition), determined from densitometry of three independent blots, are indicated.
- (E) Cell death in various cell lines with or without CQ (30  $\mu$ M).
- (F) Cell death in various cell lines with or without Prot. inhibs as in (A).

Datapoints from independent experiments are shown in (E) and (F). See also Figure S4.

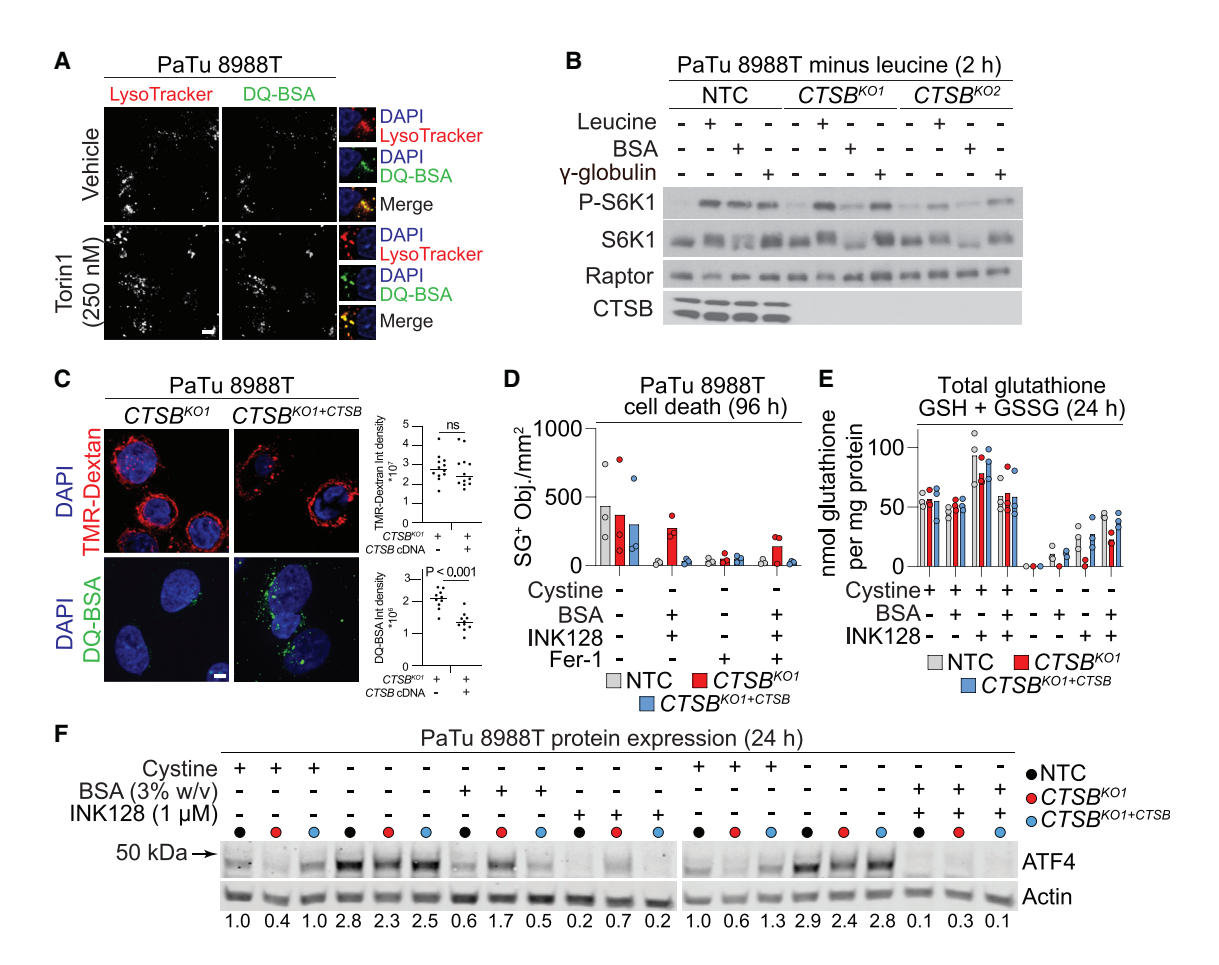


Figure 4. CTSB is required for ferroptosis suppression by extracellular albumin

(A) LysoTracker Red, a marker for lysosomes, and self-quenched BSA (DQ-BSA) fluorescence in PaTu 8988T cells. Scale bar, 5 µm.

(B) Activity of the mTORC1 signaling pathway in PaTu 8988T cells starved of leucine for 2 h and then restimulated with medium containing leucine (Leu), BSA (5% [w/v]), or γ-globulin (3% [w/v]) for 4 h. Raptor was used as a loading control.

(C) Analysis of lysosomal uptake and degradation of self-quenched BSA (DQ-BSA) in PaTu 8988T cells. The macropinocytic cargo 70-kDa tetramethylrhodamine dextran (TMR-dextran) is used to assess any effect on uptake. On the right, each datapoint represents 3 or more fields of view with 10 or more cells in total, with the median indicated by the horizontal bar. Scale bar, 5 µm. CTSB<sup>KO1</sup>, cathepsin B KO; CTSB<sup>KO1+CTSB</sup>; CTSB KO reconstituted with CTSB cDNA.

(D) Cell death determined by counting SYTOX Green-positive (SG<sup>+</sup>) dead cells. BSA, 3% (w/v). INK128, 1 μM. Fer-1, 1 μM. NTC, non-targeting CRISPR control. (E) Total GSH (GSH + GSSG), measured using Ellman's reagent after 24 h of treatment. INK128, 1 μM. BSA, 3% (w/v).

(F) Protein levels determined by western blot. Blots are representative of three independent experiments. Mean ATF4/Actin protein level ratios (normalized to the +Cys<sub>2</sub> condition), determined from densitometry of three independent blots, are indicated.

See also Figure S5.

protective effects of A+I treatment were not reversed by chloroquine or the protease inhibitor cocktail in U-2 OS<sup>N</sup> cells, indicating that non-lysosomal mechanisms of protection may also be possible in some instances (Figures 3E and 3F). However, in most cell lines, lysosome function appeared to be required for A+I treatment to protect against ferroptosis.

# Cathepsin B (CTSB) promotes albumin catabolism to suppress ferroptosis

We next sought to identify specific lysosomal protease(s) involved in albumin catabolism in the lysosome, with the hypothesis that one or more specific cathepsin enzymes would be needed for this process. For example, a recent study suggested that cathepsin L may be one important enzyme required for albumin degradation (Nofal et al., 2021). For our studies, we used pancreatic cancer cell lines, which can internalize albumin avidly

(Commisso et al., 2013) and detectably express at least 12 different lysosomal cathepsin genes (Figure S5A). To first examine albumin breakdown in the lysosome, we assessed DQ-BSA dequenching. In PaTu 8988T and MIA PaCa2 pancreatic adenocarcinoma cell lines, dequenched DQ-BSA colocalized with a lysosomal marker (LysoTracker dye), and treatment with the mTOR inhibitor Torin 1 increased lysosome numbers and dequenching of DQ-BSA, consistent with expectations and previous reports (Commisso et al., 2013; Nofal et al., 2017; Palm et al., 2015; Figure 4A). In both cell lines, DQ-BSA dequenching was suppressed by the CTSB inhibitor CA074 methyl ester but not by the cathepsin L and S inhibitor R11-OEt (van der Linden et al., 2016; Figure S5B). The CTSB inhibitor itself did not affect uptake of materials from the extracellular environment, as determined by internalization of tetramethylrhodamine (TMR)dextran (Figure S5B).

#### **Article**



Next, as a screening strategy to identify cathepsins involved in albumin catabolism, we examined the ability of extracellular albumin to restore mTOR pathway activity in cells treated with different inhibitors. Here we used leucine deprivation as a condition to basally inhibit mTOR activity (Wyant et al., 2017) because cystine deprivation does not potently inhibit mTOR activity itself over short timescales (Conlon et al., 2021). The CTSB inhibitor CA074 methyl ester prevented extracellular albumin from reactivating the mTOR pathway in leucine- and serum-deprived cells, consistent with this enzyme being required for albumin catabolism (Wyant et al., 2017; Figure S5C). CRISPR-Cas9-mediated disruption of CTSB in PaTu 8988T cells prevented albumin, but not γ-globulin, from reactivating the mTOR signaling pathway upon leucine starvation (Figure 4B). In contrast, genetic disruption of CTSL and CTSD had no effect on the ability of extracellular albumin to reactivate the mTOR pathway in leucine-deprived cells (Figures S5A and S5D). Thus, CTSB appeared to be a major albumin proteolytic enzyme in the pancreatic cancer cell lines examined here.

Based on these results, we examined PaTu 8988T non-targeting control (NTC) cells, CTSB gene-disrupted (KO1) cells, or CTSBKO1 cells where wild-type CTSB was reconstituted by gene overexpression (KO1+CTSB) (Figure S5E). With respect to albumin catabolism, we observed that CTSB reconstitution restored the dequenching of DQ-BSA that was lost in CTSB<sup>KO1</sup> cells (Figure 4C). Turning to cell death, we examined how CTSB affected the ability of A+I treatment to prevent ferroptosis in response to cystine deprivation. NTC, CTSBKO1, and CTSB<sup>KO1+CTSB</sup> cells were killed by cystine deprivation; however, although NTC and reconstituted CTSBKO1+CTSB cells were fully protected under these conditions by A+I treatment, CTSBKO1 cells were not (Figure 4D). Under conditions of cystine deprivation and A+I treatment, NTC and CTSBKO1+CTSB cells also retained higher levels of intracellular GSH than CTSBKO1 cells, as detected using Ellman's reagent or liquid chromatography coupled to mass spectrometry (Figures 4E and S5F). Albumin supplementation alone also more effectively reduced ATF4 protein accumulation and suppressed C11 BODIPY 581/591 oxidation in cystinedeprived NTC and CTSBKO1+CTSB cells than in CTSBKO1 cells (Figures 4F and S5G). These results suggested that lysosomal CTSB function was necessary for extracellular albumin to fully suppress ferroptosis in cells deprived of extracellular cystine.

#### **CTNS** is required for albumin to suppress ferroptosis

Cysteine is exported from the lysosome in the form of cystine by the transporter cystinosin (CTNS) (Gahl et al., 2002). Our results suggested that lysosomal albumin catabolism by CTSB liberated free cysteine that could be used in subsequent GSH synthesis and, thus, to suppress toxic lipid hydroperoxide accumulation. However, cysteine generated in this manner in the lysosome needs to be exported to the cytosol. Thus, we hypothesized that CTNS function would be necessary for A+I treatment to protect cells against ferroptosis. To test this hypothesis, we generated two independent clonal CTNS gene-disrupted (KO) cell lines that, because of the absence of a suitable antibody, we confirmed to be mutant by genomic DNA sequencing (STAR methods). When cultured in regular medium, unmodified control cells and CTNSKO1/2 cell lines had similar mTOR pathway activity, proliferation rates, and cell death in response to cystine deprivation (Figures 5A and S6). However, when deprived of cystine, control cells but not CTNSKO1/2 cells were protected against ferroptosis by the A+I combination (Figure 5A). Thus, CTNS appeared to be required for A+I to inhibit ferroptosis in response to cystine deprivation.

Functionally, cystine deprivation for 10 h increased lipid oxidation in control and CTNSKO1/2 cell lines (Figure 5B). Consistent with our viability results, A+I suppressed C11 oxidation after 10 h of cystine deprivation more effectively in control cells than in CTNS<sup>KO1/2</sup> cell lines (Figure 5B). However, observed differences in C11 oxidation were small at this time point; it was not possible to examine C11 oxidation at later time points after cystine deprivation because control cells would be killed under these conditions. A+I treatment less effectively maintained intracellular GSH levels in cystine-deprived CTNSKO1/2 cells compared with control cells (Figure 5C). ATF4 accumulation in response to cystine deprivation was higher in CTNS<sup>KO1/2</sup> cells compared with control cells and less effectively suppressed by albumin supplementation (Figure 5D). These data suggested that CTNS function was required for A+I treatment to support GSH synthesis and suppress ferroptosis in response to deprivation of extracellular cystine.

#### Albumin protects cell spheroids and patient-derived glioma cells from ferroptosis

Compared with cells grown in monolayers, cells grown under detached conditions more closely recapitulate the in vivo tumor microenvironment (Dixon et al., 2014; Friedrich et al., 2009; Jiang et al., 2016; Schafer et al., 2009). Accordingly, we examined whether extracellular albumin combined with mTOR inhibition could inhibit ferroptosis in HT-1080N spheroids established over the course of 3 days in ultra-low adherence vessels (Figure 6A). Because it was not possible to replace the growth medium without disturbing the spheroids, we instead triggered intracellular cystine deprivation using the small-molecule system x<sub>c</sub> inhibitor erastin2. Unexpectedly, co-treatment with albumin alone was sufficient to fully maintain HT-1080<sup>N</sup> spheroid morphology and overall viability, as assessed by total ATP levels, even without addition of mTOR inhibitor (Figures 6A and 6B). Based on previous findings (Barbone et al., 2008; Riedl et al., 2017), we hypothesized that spheroid growth may reduce mTOR signaling and obviate the need for exogenous mTOR inhibition. Indeed, HT-1080<sup>N</sup> cells grown as spheroids had reduced RPS6 phosphorylation compared with HT-1080<sup>N</sup> cell growth in monolayers (Figure 6C). Similar results for ferroptosis inhibition and mTOR pathway activity were obtained with A375<sup>N</sup> cells grown as spheroids versus in a monolayer, suggesting a generalizable effect (Figures S7A-S7C).

To extend our results, we examined human primary patientderived gliomaspheres (Mai et al., 2017). In response to erastin2 treatment, we observed a small but quantitative reduction in gliomasphere viability that was reverted by co-incubation with albumin alone (Figures 6D and 6E). Compared with HT-1080<sup>N</sup> cells grown in monolayers, which we used for comparison, gliomaspheres had decreased RPS6 phosphorylation, suggestive of reduced mTORC1 pathway activity (Figure 6F). Thus, the viability of primary cancer spheroids deprived of cystine can be supported by exogenous albumin alone, as observed in established cancer cell lines grown under similar conditions.

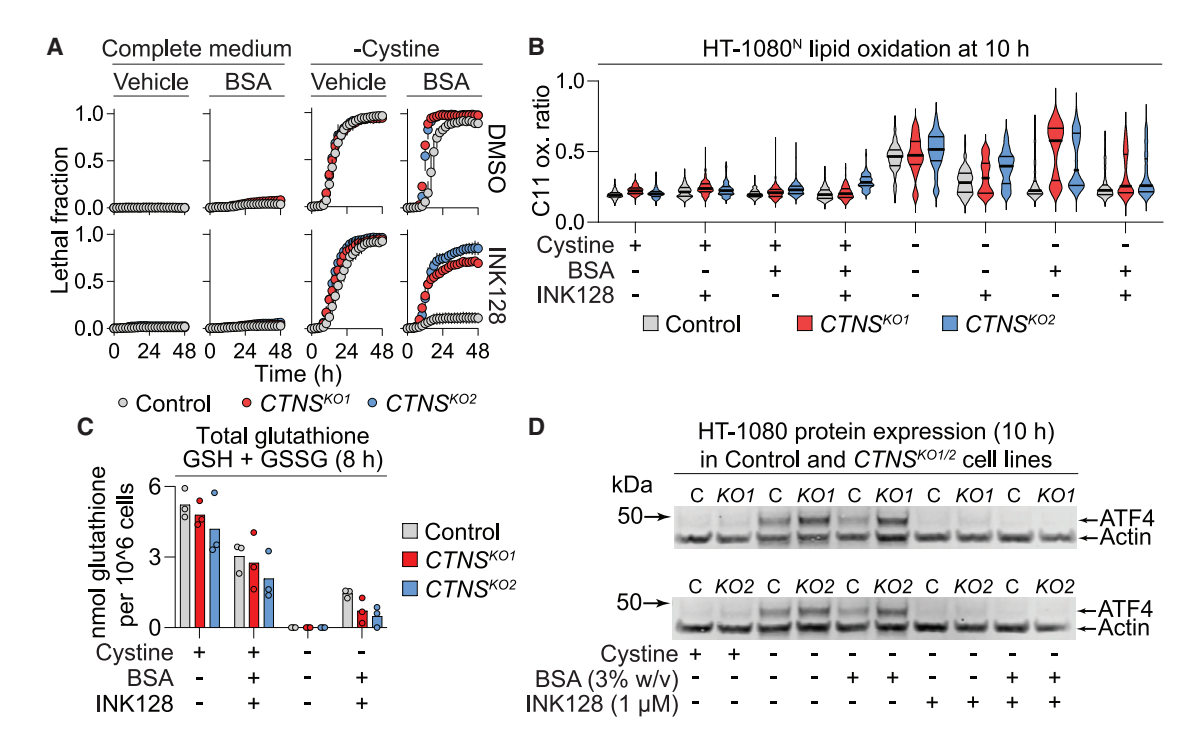


Figure 5. CTNS is required for ferroptosis suppression by extracellular albumin

(A) Cell death in HT-1080<sup>N</sup> Control or cystinosin (CTNS) gene-disrupted (KO) cell lines. INK128, 1 μM. BSA, 3% (w/v). Data represent mean ± SD from three independent experiments.

(B) C11 oxidation ratio (oxidized C11/[reduced C11 + oxidized C11]). INK128, 1 μM. BSA, 3% (w/v). Data acquired from 59–512 individual cells per condition were analyzed. Representative data from one of three independent experiments are shown.

(C) Total GSH (GSH + GSSG) measured using Ellman's reagent. INK128, 1 μM. BSA, 3% (w/v).

(D) Protein levels determined by western blot. C, control. Blots are representative of three independent experiments.

See also Figure S6.

#### **DISCUSSION**

Cysteine is required to enable cell proliferation and ward off ferroptosis in many cancer cells in vitro and in vivo (Badgley et al., 2020; Combs and DeNicola, 2019; Dixon et al., 2014). Here we define a mechanism that is active in many cancer cells that enables these cells to evade ferroptosis when extracellular cystine is absent: uptake and lysosomal catabolism of extracellular albumin. Albumin is highly abundant in serum and remarkably cysteine rich (Figure S3A). Cysteine is usually maintained at a low level in the cell compared with other amino acids (Abu-Remaileh et al., 2017). Based on our findings, we propose that serum albumin acts as an important extracellular cysteine reservoir, accessible to cells that can internalize and catabolize this protein. Along with direct uptake of cysteine (Meira et al., 2021) and induction of the cysteine-generating transsulfuration pathway (Zhu et al., 2019), the uptake and catabolism of extracellular albumin, or other proteins obtained from serum or from dead cell debris (Kim et al., 2018), is likely to be an important mechanism used by cancer cells to maintain intracellular cysteine levels when extracellular free cystine is limited (Figure 7).

Our results suggest that albumin catabolism in the lysosome by CTSB and other proteases (Nofal et al., 2021) is essential for inhibiting ferroptosis in cystine-deprived cells. Protein catabolism in the lysosome is strongly amplified by concomitant inhibition of mTORC1 (Nofal et al., 2017; Palm et al., 2015; Ratto et al., 2022), a result we confirm here. We recently reported that mTORC1 inhibition alone is sufficient to attenuate ferroptosis in cystine-deprived cells and proposed that this involves slowing of mTORC1-dependent mRNA translation, enabling diversion of available cysteine toward GSH synthesis (Conlon et al., 2021). However, effects on mRNA translation only appeared to partially account for the ability of mTORC1 inhibition to inhibit ferroptosis in these experiments. Given our present findings, we speculate that catabolism of albumin or other proteins present in standard growth medium containing 10% serum may also contribute to the ability of mTOR inhibition alone to protect from ferroptosis in response to cystine deprivation, at least under our growth conditions.

Our results indicate that protection from ferroptosis by extracellular protein requires export of newly liberated cystine from the lysosome into the cytosol via the transporter CTNS, at least in HT-1080 cells. This is consistent with an overall model where lysosomal albumin catabolism feeds cysteine to the cytosolic GSH biosynthetic machinery to maintain GPX4 activity and suppress lethal lipid peroxidation under conditions of extracellular cystine limitation. In contrast, disruption of *CTNS* has little effect on basal ferroptosis sensitivity when albumin is not present, suggesting that cystine stored in the lysosome (Abu-Remaileh et al., 2017) does not normally contribute to ferroptosis regulation. In *Drosophila melanogaster*, CTNS-dependent cystine export can



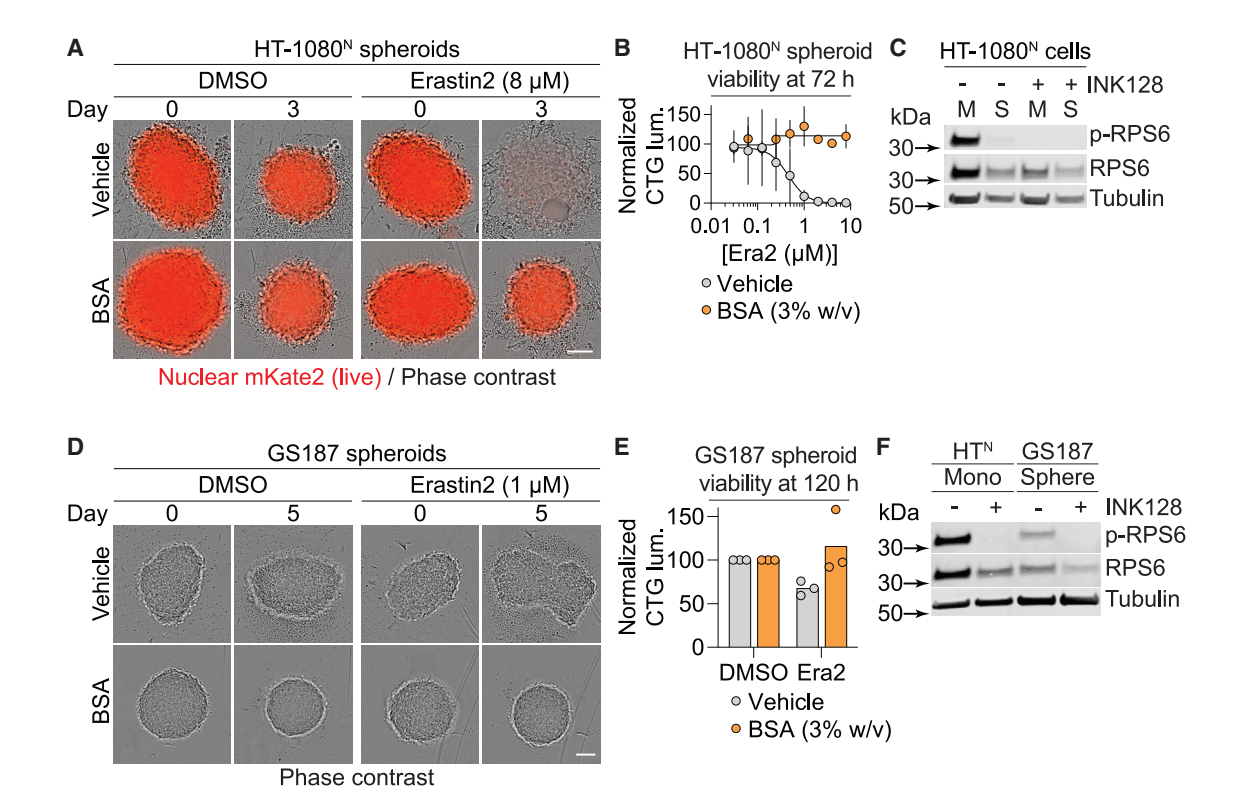


Figure 6. Albumin promotes spheroid viability in response to Cys<sub>2</sub> deprivation

(A) HT-1080<sup>N</sup> spheroids established over 3 days (day 0) prior to treatment for 3 days (day 3). BSA, 3% (w/v). Scale bar, 100 µm.

- (B) Viability of HT-1080<sup>N</sup> spheroids established and treated as in (A), determined using CellTiter-Glo.
- (C) mTOR pathway activity, assessed by western blot after 24-h treatment. M, monolayer; S, spheroid. INK128, 1 μM.
- (D) Gliomaspheres (line GS187) established over 3 days (day 0) prior to treatment for 5 days. BSA, 3% (w/v). Scale bar, 100 µm.
- (E) Viability of GS187 spheroids established and treated as in (D), determined using CellTiter-Glo.
- (F) mTOR pathway activity, assessed by western blot in HT-1080N (HTN) cells grown in monolayer (mono) or GS187 cells grown as spheroids and treated with or without INK128 (1  $\mu$ M) for 24 h.

In (A) and (D), images are representative of three independent experiments. In (B) and (E), data are mean ± SD from three independent experiments. In (C) and (F), blots are representative of three independent experiments. p-RPS6 is phosphorylated at Ser235/236. See also Figure S7.

help stimulate mTORC1 activity through a complex mechanism involving regulation of coenzyme A metabolism and Krebs cycle activity (Jouandin et al., 2022). We speculate that, in metabolically stressed cancer cells, reduced lysosomal cystine export via CTNS could attenuate mTORC1 signaling and help prime cells to use extracellular albumin to restore intracellular amino acid homeostasis.

Albumin can be internalized into cancer cells through macropinocytosis and other endocytic processes, including receptor-mediated uptake (Commisso et al., 2013; Kamphorst et al., 2015; Kim et al., 2018). Macropinocytosis is stimulated by oncogenic activation of the RAS pathway (Commisso et al., 2013). We observed that extracellular protein prevented ferroptosis in cell lines with (e.g., HT-1080) and without (e.g., T98G

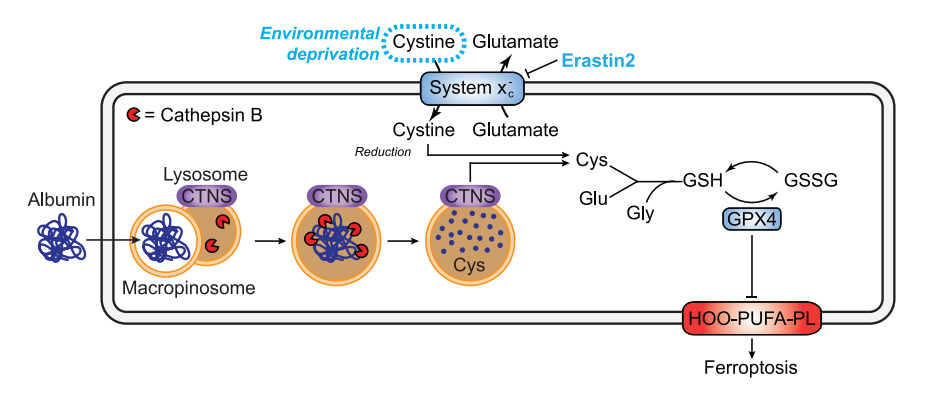


Figure 7. Model of how exogenous protein protects from ferroptosis

Ingestion and lysosomal catabolism of albumin liberates free cysteine/cystine that can be exported to the cytosol for the synthesis of antiferroptotic metabolites like GSH. Extracellular albumin may enter the cell via macropinocytosis but other routes of albumin entry and trafficking to lysosomes are also possible.



### Cell Chemical Biology Article

and U-2 OS) RAS pathway mutations. It is possible that macropinocytosis is active in non-RAS pathway mutant cell lines for other reasons, or that distinct mechanisms contribute to protein uptake in these cells. Albumin taken into the cell by whatever means is routed to the lysosome, where in most cases catabolism of this protein can supply the cell with cysteine needed to synthesize GSH and possibly other protective sulfur-containing metabolites, block lipid peroxidation, and prevent the onset of ferroptosis.

#### **Limitations of the study**

The combination of albumin and mTOR inhibition suppresses ferroptosis in most cystine-deprived cancer cell lines through a mechanism that involves lysosomal protein catabolism. However, in U-2 OS cells, the protective effect of A+I treatment was not lost upon pharmacological inhibition of lysosomal function. It is possible that other mechanisms of albumin-mediated protection against ferroptosis, such as a direct antioxidant effect or facilitated import of anti-ferroptotic molecules, are more important mediators or ferroptosis resistance in some cell lines. This study also does not address the potential role of albumin in maintaining intracellular cysteine homeostasis in non-cancer cells. Slc7a11 knockout mice lacking system x<sub>c</sub><sup>-</sup> function are viable and exhibit only minor phenotypes, especially in comparison with animals lacking Gpx4 (Friedmann Angeli et al., 2014; Sato et al., 2005). Along with direct cysteine uptake (Meira et al., 2021), it is possible that the uptake and catabolism of albumin or other cysteine-rich extracellular proteins reduces the dependence of cells in the body on system x<sub>c</sub><sup>-</sup>-mediated cystine import for survival.

#### **SIGNIFICANCE**

Whether disruption of cystine import can be exploited therapeutically for cancer treatment remains unclear. Numerous cancers overexpress SLC7A11 (Koppula et al., 2021). While drug-like small molecule system x<sub>c</sub> inhibitors and extracellular cystinedegrading enzymes (e.g., cyst[e]inase) can slow tumor growth in vivo, these agents do not appear to cause consistent tumor regression (Cramer et al., 2017; Zhang et al., 2019). Our results, together with other recent findings from sorafenib-treated cancer cells (Byun et al., 2022), suggest a possible explanation for this observation: that uptake and catabolism of albumin compensates for limited extracellular free cystine to inhibit ferroptosis in vivo. Cells growing under detached conditions have reduced levels of mTOR activity (Barbone et al., 2008; Riedl et al., 2017), which could further favor lysosomal protein catabolism and enhance this protective mechanism in tumors. Our results suggest that induction of ferroptosis in vivo by cystine deprivation regimens may be augmented by concomitant inhibition of protein uptake from the extracellular environment or lysosome-mediated albumin catabolism.

#### **STAR**\*METHODS

Detailed methods are provided in the online version of this paper and include the following:

- KEY RESOURCES TABLE
- RESOURCE AVAILABILITY

- Lead contact
- Materials availability
- Data and code availability
- EXPERIMENTAL MODELS AND SUBJECT DETAILS
  - Cell lines and culture conditions
- METHOD DETAILS
  - Chemicals
  - Amino acid deprivation and protein supplementation media
  - Cell death and proliferation tracking
  - Glutathione quantification via Ellman's reagent
  - Glutathione quantification via mass spectrometry
  - C11 BODIPY 581/591 imaging
  - DQ-BSA imaging
  - Western blotting
  - Virus generation and use
  - mTORC1 and mTORC2 shRNA-mediated gene silencing
  - O CRISPR/Cas9 genome editing
  - Spheroid cell culture and experiments
- QUANTIFICATION AND STATISTICAL ANALYSIS

#### SUPPLEMENTAL INFORMATION

Supplemental information can be found online at https://doi.org/10.1016/j.chembiol.2022.10.006.

#### **ACKNOWLEDGMENTS**

We thank R. Skouta, Z. Inde, I. Ulengin-Talkish, I. Foe, C. Gottlieb, K.C. Farrell, T. Stearns, M. Bogyo, and R. Perera for equipment, reagents, and help with experiments; K. Galenkamp and C. Commisso for advice; and L. Pope and L. Magtanong for comments on the manuscript. This work was supported by the Department of Defence (DODW81XWH-20-1-0453 to D.A.A.), NIH (T32GM007276 to D.A.A., DP2-CA271386 to M.A.-R., 1R01GM122923 to S.J.D., and R01NS121319 to D.A.A., and S.J.D.) and by the American Cancer Society (RSG-21-017-01-CCG to S.J.D.).

#### **AUTHOR CONTRIBUTIONS**

Conceptualization, D.A.A., N.N.L., M. A.-R., and S.J.D.; methodology, D.A.A., N.N.L., W.D., D.M., D.A.N., M.A.-R., and S.J.D.; investigation, D.A.A., N.N.L., G.A., W.D., and C.A.P.; writing – original draft, D.A.A., N.N.L., D.A.N., M.A.-R., and S.J.D.; resources, D.A.N., M.A.-R., and S.J.D.; supervision, D.A.N., M.A.-R., and S.J.D.

#### **DECLARATION OF INTERESTS**

D.A.N. is a co-founder of Trethera Corporation and Katmai Pharmaceuticals and has equity in those companies and in Sofie Biosciences. M.A.-R. is a scientific advisory board member of Lycia Therapeutics. S.J.D. is a co-founder of Prothegen Inc., a member of the scientific advisory board for Ferro Therapeutics and Hillstream BioPharma, and an inventor on patents related to ferroptosis.

Received: March 14, 2022 Revised: September 1, 2022 Accepted: October 5, 2022 Published: October 27, 2022

#### **REFERENCES**

Abu-Remaileh, M., Wyant, G.A., Kim, C., Laqtom, N.N., Abbasi, M., Chan, S.H., Freinkman, E., and Sabatini, D.M. (2017). Lysosomal metabolomics

#### **Article**



reveals V-ATPase- and mTOR-dependent regulation of amino acid efflux from lysosomes. Science 358, 807-813.

Badgley, M.A., Kremer, D.M., Maurer, H.C., DelGiorno, K.E., Lee, H.J., Purohit, V., Sagalovskiy, I.R., Ma, A., Kapilian, J., Firl, C.E.M., et al. (2020). Cysteine depletion induces pancreatic tumor ferroptosis in mice. Science 368, 85-89.

Barbone, D., Yang, T.M., Morgan, J.R., Gaudino, G., and Broaddus, V.C. (2008). Mammalian target of rapamycin contributes to the acquired apoptotic resistance of human mesothelioma multicellular spheroids. J. Biol. Chem. 283, 13021-13030.

Bartolacci, C., Andreani, C., Vale, G., Berto, S., Melegari, M., Crouch, A.C., Baluya, D.L., Kemble, G., Hodges, K., Starrett, J., et al. (2022). Targeting de novo lipogenesis and the Lands cycle induces ferroptosis in KRAS-mutant lung cancer. Nat. Commun. 13, 4640.

Bersuker, K., Hendricks, J.M., Li, Z., Magtanong, L., Ford, B., Tang, P.H., Roberts, M.A., Tong, B., Maimone, T.J., Zoncu, R., et al. (2019). The CoQ oxidoreductase FSP1 acts parallel to GPX4 to inhibit ferroptosis. Nature 575 688-692

Byun, J.K., Lee, S., Kang, G.W., Lee, Y.R., Park, S.Y., Song, I.S., Yun, J.W., Lee, J., Choi, Y.K., and Park, K.G. (2022). Macropinocytosis is an alternative pathway of cysteine acquisition and mitigates sorafenib-induced ferroptosis in hepatocellular carcinoma. J. Exp. Clin. Cancer Res. 41, 98.

Cantin, A.M., Paquette, B., Richter, M., and Larivée, P. (2000). Albumin-mediated regulation of cellular glutathione and nuclear factor kappa B activation. Am. J. Respir. Crit. Care Med. 162, 1539-1546.

Carballal, S., Radi, R., Kirk, M.C., Barnes, S., Freeman, B.A., and Alvarez, B. (2003). Sulfenic acid formation in human serum albumin by hydrogen peroxide and peroxynitrite. Biochemistry 42, 9906-9914.

Choi, S., Choi, E.Y., Kim, D.J., Kim, J.H., Kim, T.S., and Oh, S.W. (2004). A rapid, simple measurement of human albumin in whole blood using a fluorescence immunoassay (I). Clin. Chim. Acta 339, 147-156.

Combs, J.A., and DeNicola, G.M. (2019). The non-essential amino acid cysteine becomes essential for tumor proliferation and survival. Cancers

Commisso, C., Davidson, S.M., Soydaner-Azeloglu, R.G., Parker, S.J., Kamphorst, J.J., Hackett, S., Grabocka, E., Nofal, M., Drebin, J.A., Thompson, C.B., et al. (2013). Macropinocytosis of protein is an amino acid supply route in Ras-transformed cells. Nature 497, 633-637.

Conlon, M., Poltorack, C.D., Forcina, G.C., Armenta, D.A., Mallais, M., Perez, M.A., Wells, A., Kahanu, A., Magtanong, L., Watts, J.L., et al. (2021). A compendium of kinetic modulatory profiles identifies ferroptosis regulators. Nat. Chem. Biol. 17, 665-674.

Cramer, S.L., Saha, A., Liu, J., Tadi, S., Tiziani, S., Yan, W., Triplett, K., Lamb, C., Alters, S.E., Rowlinson, S., et al. (2017). Systemic depletion of L-cyst(e)ine with cyst(e)inase increases reactive oxygen species and suppresses tumor growth. Nat. Med. 23, 120-127.

Davidson, S.M., Jonas, O., Keibler, M.A., Hou, H.W., Luengo, A., Mayers, J.R., Wyckoff, J., Del Rosario, A.M., Whitman, M., Chin, C.R., et al. (2017). Direct evidence for cancer-cell-autonomous extracellular protein catabolism in pancreatic tumors. Nat. Med. 23, 235-241.

Dixon, S.J., Lemberg, K.M., Lamprecht, M.R., Skouta, R., Zaitsev, E.M., Gleason, C.E., Patel, D.N., Bauer, A.J., Cantley, A.M., Yang, W.S., et al. (2012). Ferroptosis: an iron-dependent form of nonapoptotic cell death. Cell 149, 1060-1072.

Dixon, S.J., Patel, D.N., Welsch, M., Skouta, R., Lee, E.D., Hayano, M., Thomas, A.G., Gleason, C.E., Tatonetti, N.P., Slusher, B.S., and Stockwell, B.R. (2014). Pharmacological inhibition of cystine-glutamate exchange induces endoplasmic reticulum stress and ferroptosis. Elife 3, e02523.

Doll, S., Freitas, F.P., Shah, R., Aldrovandi, M., da Silva, M.C., Ingold, I., Goya Grocin, A., Xavier da Silva, T.N., Panzilius, E., Scheel, C.H., et al. (2019). FSP1 is a glutathione-independent ferroptosis suppressor. Nature 575, 693-698.

Eagle, H. (1959). Amino acid metabolism in mammalian cell cultures. Science 130, 432-437.

Eagle, H., Oyama, V.I., and Piez, K.A. (1960). The reversible binding of halfcystine residues to serum protein, and its bearing on the cystine requirement of cultured mammalian cells. J. Biol. Chem. 235, 1719-1726.

Forcina, G.C., Conlon, M., Wells, A., Cao, J.Y., and Dixon, S.J. (2017). Systematic quantification of population cell death kinetics in mammalian cells. Cell Syst. 4, 600-610.e6.

Friedmann Angeli, J.P., Schneider, M., Proneth, B., Tyurina, Y.Y., Tyurin, V.A., Hammond, V.J., Herbach, N., Aichler, M., Walch, A., Eggenhofer, E., et al. (2014). Inactivation of the ferroptosis regulator Gpx4 triggers acute renal failure in mice. Nat. Cell Biol. 16, 1180-1191.

Friedrich, J., Seidel, C., Ebner, R., and Kunz-Schughart, L.A. (2009). Spheroidbased drug screen: considerations and practical approach. Nat. Protoc. 4, 309-324

Gahl, W.A., Thoene, J.G., and Schneider, J.A. (2002). Cystinosis. N. Engl. J. Med. 347, 111-121.

Geyer, P.E., Kulak, N.A., Pichler, G., Holdt, L.M., Teupser, D., and Mann, M. (2016). Plasma proteome profiling to assess human health and disease. Cell Syst. 2, 185-195.

Hangauer, M.J., Viswanathan, V.S., Ryan, M.J., Bole, D., Eaton, J.K., Matov, A., Galeas, J., Dhruv, H.D., Berens, M.E., Schreiber, S.L., et al. (2017). Drugtolerant persister cancer cells are vulnerable to GPX4 inhibition. Nature 551, 247-250.

Inde, Z., Rodencal, J., and Dixon, S.J. (2021). Quantification of drug-induced fractional killing using high-throughput microscopy. STAR Protoc. 2, 100300. Ingold, I., Berndt, C., Schmitt, S., Doll, S., Poschmann, G., Buday, K., Roveri, A., Peng, X., Porto Freitas, F., Seibt, T., et al. (2018). Selenium utilization by GPX4 is required to prevent hydroperoxide-induced ferroptosis. Cell 172, 409-422.e21.

Jayashankar, V., and Edinger, A.L. (2020). Macropinocytosis confers resistance to therapies targeting cancer anabolism. Nat. Commun. 11, 1121.

Jiang, L., Shestov, A.A., Swain, P., Yang, C., Parker, S.J., Wang, Q.A., Terada, L.S., Adams, N.D., McCabe, M.T., Pietrak, B., et al. (2016). Reductive carboxylation supports redox homeostasis during anchorage-independent growth. Nature 532, 255-258.

Jiang, X., Stockwell, B.R., and Conrad, M. (2021). Ferroptosis: mechanisms, biology and role in disease. Nat. Rev. Mol. Cell Biol. 22, 266-282.

Jouandin, P., Marelja, Z., Shih, Y.H., Parkhitko, A.A., Dambowsky, M., Asara, J.M., Nemazanyy, I., Dibble, C.C., Simons, M., and Perrimon, N. (2022). Lysosomal cystine mobilization shapes the response of TORC1 and tissue growth to fasting. Science 375, eabc4203.

Kamphorst, J.J., Nofal, M., Commisso, C., Hackett, S.R., Lu, W., Grabocka, E., Vander Heiden, M.G., Miller, G., Drebin, J.A., Bar-Sagi, D., et al. (2015). Human pancreatic cancer tumors are nutrient poor and tumor cells actively scavenge extracellular protein. Cancer Res. 75, 544-553.

Keyser, J.W., Fifield, R., and Watkins, G.L. (1981). Standardization of immunochemical determinations of serum albumin. Clin. Chem. 27, 736-738.

Kim, S.M., Nguyen, T.T., Ravi, A., Kubiniok, P., Finicle, B.T., Jayashankar, V., Malacrida, L., Hou, J., Robertson, J., Gao, D., et al. (2018). PTEN deficiency and AMPK activation promote nutrient scavenging and anabolism in prostate cancer cells. Cancer Discov. 8, 866-883.

Koppula, P., Lei, G., Zhang, Y., Yan, Y., Mao, C., Kondiparthi, L., Shi, J., Liu, X., Horbath, A., Das, M., et al. (2022). A targetable CoQ-FSP1 axis drives ferroptosis- and radiation-resistance in KEAP1 inactive lung cancers. Nat. Commun.

Koppula, P., Zhuang, L., and Gan, B. (2021). Cystine transporter SLC7A11/ xCT in cancer: ferroptosis, nutrient dependency, and cancer therapy. Protein Cell 12, 599-620.

Leu, J.I.J., Murphy, M.E., and George, D.L. (2019). Mechanistic basis for impaired ferroptosis in cells expressing the African-centric S47 variant of p53. Proc. Natl. Acad. Sci. USA 116, 8390-8396.

Magtanong, L., Ko, P.J., To, M., Cao, J.Y., Forcina, G.C., Tarangelo, A., Ward, C.C., Cho, K., Patti, G.J., Nomura, D.K., et al. (2019). Exogenous monounsaturated fatty acids promote a ferroptosis-resistant cell state. Cell Chem. Biol. 26, 420-432.e9.



Mai, W.X., Gosa, L., Daniels, V.W., Ta, L., Tsang, J.E., Higgins, B., Gilmore, W.B., Bayley, N.A., Harati, M.D., Lee, J.T., et al. (2017). Cytoplasmic p53 couples oncogene-driven glucose metabolism to apoptosis and is a therapeutic target in glioblastoma. Nat. Med. 23, 1342-1351.

Meira, W., Daher, B., Parks, S.K., Cormerais, Y., Durivault, J., Tambutte, E., Pouyssegur, J., and Vučetić, M. (2021). A cystine-cysteine intercellular shuttle prevents ferroptosis in xCT(KO) pancreatic ductal adenocarcinoma cells. Cancers 13, 1434.

Neuzil, J., Gebicki, J.M., and Stocker, R. (1993). Radical-induced chain oxidation of proteins and its inhibition by chain-breaking antioxidants. Biochem. J. 293 (Pt 3), 601-606.

Nofal, M., Wang, T., Yang, L., Jankowski, C.S.R., Hsin-Jung Li, S., Han, S., Parsons, L., Frese, A.N., Gitai, Z., Anthony, T.G., et al. (2021). GCN2 adapts protein synthesis to scavenging-dependent growth. Cell Syst. 13, 158-172.e9.

Nofal, M., Zhang, K., Han, S., and Rabinowitz, J.D. (2017). mTOR inhibition restores amino acid balance in cells dependent on catabolism of extracellular protein. Mol. Cell 67, 936-946.e5.

Palm, W. (2019). Metabolic functions of macropinocytosis. Philos. Trans. R. Soc. Lond. B Biol. Sci. 374, 20180285.

Palm, W., Park, Y., Wright, K., Pavlova, N.N., Tuveson, D.A., and Thompson, C.B. (2015). The utilization of extracellular proteins as nutrients is suppressed by mTORC1. Cell 162, 259-270.

Park, Y., Reyna-Neyra, A., Philippe, L., and Thoreen, C.C. (2017). mTORC1 balances cellular amino acid supply with demand for protein synthesis through post-transcriptional control of ATF4. Cell Rep. 19, 1083-1090.

Perera, R.M., Stoykova, S., Nicolay, B.N., Ross, K.N., Fitamant, J., Boukhali, M., Lengrand, J., Deshpande, V., Selig, M.K., Ferrone, C.R., et al. (2015). Transcriptional control of autophagy-lysosome function drives pancreatic cancer metabolism. Nature 524, 361-365.

Poltorack, C.D., and Dixon, S.J. (2021). Understanding the role of cysteine in ferroptosis: progress & paradoxes. FEBS J. 289, 374-385.

Poole, B., and Ohkuma, S. (1981). Effect of weak bases on the intralysosomal pH in mouse peritoneal macrophages. J. Cell Biol. 90, 665-669.

Ratto, E., Chowdhury, S.R., Siefert, N.S., Schneider, M., Wittmann, M., Helm, D., and Palm, W. (2022). Direct control of lysosomal catabolic activity by mTORC1 through regulation of V-ATPase assembly. Nat. Commun. 13, 4848.

Reis, R.C., Sorgine, M.H., and Coelho-Sampaio, T. (1998). A novel methodology for the investigation of intracellular proteolytic processing in intact cells. Eur. J. Cell Biol. 75, 192-197.

Riedl, A., Schlederer, M., Pudelko, K., Stadler, M., Walter, S., Unterleuthner, D., Unger, C., Kramer, N., Hengstschläger, M., Kenner, L., et al. (2017). Comparison of cancer cells in 2D vs 3D culture reveals differences in AKTmTOR-S6K signaling and drug responses. J. Cell Sci. 130, 203-218.

Sato, H., Shiiya, A., Kimata, M., Maebara, K., Tamba, M., Sakakura, Y., Makino, N., Sugiyama, F., Yagami, K.i., Moriguchi, T., et al. (2005). Redox imbalance in cystine/glutamate transporter-deficient mice. J. Biol. Chem. 280. 37423-37429.

Schafer, Z.T., Grassian, A.R., Song, L., Jiang, Z., Gerhart-Hines, Z., Irie, H.Y., Gao, S., Puigserver, P., and Brugge, J.S. (2009). Antioxidant and oncogene rescue of metabolic defects caused by loss of matrix attachment. Nature *461*, 109–113.

Schneider, C.A., Rasband, W.S., and Eliceiri, K.W. (2012). NIH Image to ImageJ: 25 years of image analysis. Nat. Methods 9, 671-675. https://doi. org/10.1038/nmeth.2089.

Shimada, K., Skouta, R., Kaplan, A., Yang, W.S., Hayano, M., Dixon, S.J., Brown, L.M., Valenzuela, C.A., Wolpaw, A.J., and Stockwell, B.R. (2016). Global survey of cell death mechanisms reveals metabolic regulation of ferroptosis. Nat. Chem. Biol. 12, 497-503.

Sullivan, M.R., Danai, L.V., Lewis, C.A., Chan, S.H., Gui, D.Y., Kunchok, T., Dennstedt, E.A., Vander Heiden, M.G., and Muir, A. (2019). Quantification of microenvironmental metabolites in murine cancers reveals determinants of tumor nutrient availability. Elife 8, e44235.

Tarangelo, A., Magtanong, L., Bieging-Rolett, K.T., Li, Y., Ye, J., Attardi, L.D., and Dixon, S.J. (2018). p53 suppresses metabolic stress-induced ferroptosis in cancer cells. Cell Rep. 22, 569-575.

Tarangelo, A., Rodencal, J., Kim, J.T., Magtanong, L., Long, J.Z., and Dixon, S.J. (2022). Nucleotide biosynthesis links glutathione metabolism to ferroptosis sensitivity. Life Sci. Alliance 5. e202101157.

van der Linden, W.A., Schulze, C.J., Herbert, A.S., Krause, T.B., Wirchnianski, A.A., Dye, J.M., Chandran, K., and Bogyo, M. (2016). Cysteine cathepsin inhibitors as anti-ebola agents. ACS Infect. Dis. 2, 173-179.

Viswanathan, V.S., Ryan, M.J., Dhruv, H.D., Gill, S., Eichhoff, O.M., Seashore-Ludlow, B., Kaffenberger, S.D., Eaton, J.K., Shimada, K., Aguirre, A.J., et al. (2017). Dependency of a therapy-resistant state of cancer cells on a lipid peroxidase pathway. Nature 547, 453-457.

Wang, T., Birsoy, K., Hughes, N.W., Krupczak, K.M., Post, Y., Wei, J.J., Lander, E.S., and Sabatini, D.M. (2015). Identification and characterization of essential genes in the human genome. Science 350, 1096-1101.

Wang, W., Green, M., Choi, J.E., Gijón, M., Kennedy, P.D., Johnson, J.K., Liao, P., Lang, X., Kryczek, I., Sell, A., et al. (2019). CD8(+) T cells regulate tumour ferroptosis during cancer immunotherapy. Nature 569, 270-274.

Wortel, I.M.N., van der Meer, L.T., Kilberg, M.S., and van Leeuwen, F.N. (2017). Surviving stress: modulation of ATF4-mediated stress responses in normal and malignant cells. Trends Endocrinol. Metab. 28, 794-806.

Wyant, G.A., Abu-Remaileh, M., Wolfson, R.L., Chen, W.W., Freinkman, E., Danai, L.V., Vander Heiden, M.G., and Sabatini, D.M. (2017). mTORC1 activator SLC38A9 is required to efflux essential amino acids from lysosomes and use protein as a nutrient. Cell 171, 642-654.e12.

Yang, W.S., SriRamaratnam, R., Welsch, M.E., Shimada, K., Skouta, R., Viswanathan, V.S., Cheah, J.H., Clemons, P.A., Shamji, A.F., Clish, C.B., et al. (2014). Regulation of ferroptotic cancer cell death by GPX4. Cell 156,

Zhang, Y., and Commisso, C. (2019). Macropinocytosis in cancer: a complex signaling network. Trends Cancer 5, 332-334.

Zhang, Y., Tan, H., Daniels, J.D., Zandkarimi, F., Liu, H., Brown, L.M., Uchida, K., O'Connor, O.A., and Stockwell, B.R. (2019). Imidazole ketone erastin induces ferroptosis and slows tumor growth in a mouse lymphoma model. Cell Chem. Biol. 26, 623-633.e9.

Zhu, J., Berisa, M., Schwörer, S., Qin, W., Cross, J.R., and Thompson, C.B. (2019). Transsulfuration activity can support cell growth upon extracellular cysteine limitation. Cell Metab. 30, 865-876.e5.

# **Cell Chemical Biology Article**



#### **STAR**\***METHODS**

#### **KEY RESOURCES TABLE**

REAGENT or RESOURCE	SOURCE	IDENTIFIER
Antibodies		
4E-BP1	Cell Signaling Technology	Cat# 9644; RRID: AB_2097841
GAPDH	Cell Signaling Technology	Cat# 2118; RRID: AB_561053
Phospho-4EB-P1 (Thr37/46)	Cell Signaling Technology	Cat# 9459; RRID: AB_330985
Phospho-RPS6 (Ser235/236)	Cell Signaling Technology	Cat# 4858; RRID: AB_916156
RPS6	Cell Signaling Technology	Cat# 2217; RRID: AB_331355
Alpha-tubulin, clone DM1A	Fisher Scientific	Cat# MS581P1
SP1	Proteintech	Cat# 20886-1-AP, RRID: AB_2878756
GPX4	Abcam	Cat# ab125066, RRID: AB_10973901
CTSL	Abcam	Cat# ab200738
TFRC	Thermo Fisher Scientific	Cat# 13-6800, RRID: AB_2533029
Beta-Actin	Santa Cruz Biotechnology	Cat# sc-47778, RRID: AB_626632
p53	Santa Cruz Biotechnology	Cat# sc-126, RRID: AB_628082
Rb	BD Biosciences	Cat# 554136, RRID: AB_395259
Raptor	Millipore Sigma	Cat# 09-217, RRID: AB_612103
Phospho-S6K1 (Thr389)	Cell Signaling Technology	Cat# 9234, RRID: AB_2269803
S6K1	Cell Signaling Technology	Cat# 2708, RRID: AB_390722
Phospho-RPS6 (Ser235/236)	Cell Signaling Technology	Cat# 4858, RRID: AB_916156
RPS6	Cell Signaling Technology	Cat# 2217, RRID: AB_331355
Phospho-4E-BP1 (Thr37/46)	Cell Signaling Technology	Cat# 9459; RRID: AB 330985
4E-BP1	Cell Signaling Technology	Cat# 9644, RRID: AB_2097841
Phospho-Rb	Cell Signaling Technology	Cat# 8516, RRID: AB_11178658
Phospho-Akt (Thr308)	Cell Signaling Technology	Cat# 4056, RRID: AB_331163
Akt	Cell Signaling Technology	Cat# 9272, RRID: AB_329827
JLK1	Cell Signaling Technology	Cat# 6439, RRID: AB_11178933
CTSB	Cell Signaling Technology	Cat# 31718, RRID: AB_2687580
CTSD	Cell Signaling Technology	Cat# 2284, RRID: AB_10694258
ATF-4	Cell Signaling Technology	Cat# 11815, RRID: AB_2616025
IRP2	Cell Signaling Technology	Cat# 37135, RRID: AB_2799110
ATG7	Cell Signaling Technology	Cat# 2631, RRID: AB_2227783
GAPDH	Cell Signaling Technology	Cat# 2118, RRID: AB_561053
LC3B	Cell Signaling Technology	Cat# 2775, RRID: AB_915950
680LT Donkey-anti-mouse	LI-COR	Cat# 926-68022, RRID: AB_10715072
680LT Donkey-anti-rabbit	LI-COR	Cat# 926-68023, RRID: AB_10706167
800CW Donkey-anti-mouse	LI-COR	Cat# 926-32212, RRID: AB_621847
800CW Donkey-anti-rabbit	LI-COR	Cat# 926-32213, RRID: AB_621848
Chemicals, peptides, and recombinant p		.,
SYTOX Green	Molecular Probes	Cat# S7020
INK128	Selleck Chemical	Cat# S2811
Bovine serum albumin	Gemini Bio-Products	Cat# 700-100P
Bovine serum albumin	Sigma Aldrich	Cat# A3294
Dimethyl Sulfoxide	Sigma-Aldrich	Cat# 276855, CAS: 67-68-5
Ferrostatin-1	Sigma-Aldrich	Cat# SML0583, CAS: 347174-05-4
Q-VD-OPh	Fisher Scientific	Cat# OPH00101M
Torin 1	i ionor odionullo	Cat# 10997

(Continued on next page)



Continued		
REAGENT or RESOURCE	SOURCE	IDENTIFIER
Rapamycin	Fisher Scientific	Cat# BP2963-1
Erastin2	Custom synthesis	N/A
Bortezomib	Fisher Scientific	Cat# NC0587961, CAS: 179324-69-7
Camptothecin	Fisher Scientific	Cat# AC276721000, CAS: 7689-03-4
CIL56	Shimada et al. (2016)	N/A
FIN56	Shimada et al. (2016)	N/A
Staurosporine	Sigma-Aldrich	Cat# S6942, CAS: 62996-74-1
/inblastine	Selleck Chemical	Cat# S1248, CAS: 143-67-9
Palbociclib	Selleck Chemical	Cat# S1116
Deferoxamine mesylate	Cayman Chemical	Cat# 14595, CAS: 138-14-7
C11 BODIPY 581/591 (4,4-difluoro- 5-(4-phenyl-1,3-butadienyl)-4-bora-3a, 4a-diaza-s-indacene-3- undecanoic acid	Molecular Probes	Cat# D3861
Methanol	Sigma-Aldrich	Cat# 34860, CAS: 67-56-1
Hoechst 33258	Thermo Fisher Scientific	Cat# H3569
ML162	Custom synthesis	
Pepstatin A	Sigma-Aldrich	Cat# P5318
eupeptin Hydrochloride	Sigma-Aldrich	Cat# L9783
E-64	Sigma-Aldrich	Cat# E3132
Chloroquine Diphosphate	Sigma-Aldrich	Cat# C6628
OQ-BSA	Invitrogen	Cat# D1205
Ovalbumin	A.G. Scientific	Cat# O-2577
Casein	EMD Millipore	Cat# 218680
Glutathione quantification assay kit	Cayman Chemical	Cat# 703002
Buthionine sulfoxamine	Thermo Fisher Scientific	Cat# AC23552-001
Nutlin-3	Selleck Chemical	Cat# S1061
CA074-Me	Gift from Matthew Bogyo, Stanford University School of Medicine	
R11-OEt	Gift from Matthew Bogyo, Stanford University School of Medicine	
_ysoTracker Red	Invitrogen	Cat# L7528
MR-Dextran	Invitrogen	Cat# D12050
r-globulin	Fisher scientific	Cat# ICN19147805
Deposited data		
Unprocessed western blots	Dixon, Scott (2022), "Ferroptosis Inhibition by Lysosome-Dependent Catabolism of Extracellular Protein", Mendeley Data, V1.	https://doi.org/10.17632/988sm4nsdx.
Experimental models: Cell lines		
Human: HT-1080	ATCC	Cat# CCL-121, RRID:CVCL_0317
Human: HT-1080 <sup>N</sup>	Forcina et al., 2017	N/A
Human: H1299 <sup>N</sup>	Tarangelo et al., 2018	N/A
Human: U-2 OS <sup>N</sup>	Forcina et al., 2017	N/A
Human: H23 <sup>Cas9,N</sup>	Inde et al., 2021	N/A
Human: A375 <sup>N</sup>	Conlon et al., 2021	N/A
Human: T98G <sup>N</sup>	Forcina et al., 2017	N/A
Human: PaTu 8988T	Gift from Rushika Perera, University of California San Francisco	N/A
Human: PaTu 8988 <i>ATG7</i> KO1	This paper	N/A
Human: PaTu 8988 ATG7 KO2	This paper	N/A
Human: PaTu 8988 <i>ATG7</i> KO3	This paper	N/A
	. J J.	

(Continued on next page)





Continued				
REAGENT or RESOURCE	SOURCE	IDENTIFIER		
Human: MIA PaCa2	Gift from Rushika Perera, University of California San Francisco	N/A		
Human: PaTu 8988 CTSB KO1	This paper	N/A		
Human: PaTu 8988 CTSB KO2	This paper	N/A		
Human: PaTu 8988 CTSD KO1	This paper	N/A		
Human: PaTu 8988 CTSD KO2	This paper	N/A		
Human: PaTu 8988 CTSL KO1	This paper	N/A		
Human: PaTu 8988 CTSL KO2	This paper	N/A		
Oligonucleotides				
See Table S1.				
Recombinant DNA				
IncuCyte NucLight Red Lentivirus Reagent (EF-1 a, Puro)	Essen BioScience	Cat# 4625		
shScramble	Addgene	Cat# 1864		
sh <i>RPTOR</i>	Addgene	Cat# 1858		
shRICTOR	Addgene	Cat# 1853		
Software and algorithms				
GraphPad Prism 9.0.1	GraphPad Software, Inc.	https://www.graphpad.com/		
Microsoft Excel 16.45	Microsoft Corporation	N/A		
ImageJ 1.52q	Schneider et al., 2012	https://imagej.nih.gov/ij		
R	https://www.r-project.org/	Version R-4.0.5		
RStudio	https://www.rstudio.com/products/ rstudio/download/	Version 1.4.1106		
Other				
ImageJ DQ-BSA processing script	Dixon, Scott (2022), "Ferroptosis Inhibition by Lysosome-Dependent Catabolism of Extracellular Protein", Mendeley Data, V1.	https://doi.org/10.17632/988sm4nsdx.7		
R program for protein cysteine abundance calculation	Dixon, Scott (2022), "Ferroptosis Inhibition by Lysosome-Dependent Catabolism of Extracellular Protein", Mendeley Data, V1.	https://doi.org/10.17632/988sm4nsdx.		

#### RESOURCE AVAILABILITY

#### **Lead contact**

Further information and requests for resources and reagents should be directed to and will be fulfilled by the Lead Contact, Scott Dixon (sjdixon@stanford.edu).

#### **Materials availability**

Plasmids, cell lines and other materials generated in this study will be shared by the lead contact upon request.

#### **Data and code availability**

- Uncropped western blot images reported in have been deposited at Mendeley and are publicly available as of the date of publication. The DOI is listed in the key resources table.
- One ImageJ script used to analyze DQ-BSA puncta and one R program used to analyze cysteine abundance in proteins have been deposited to Mendeley and are publicly available as of the date of publication. The DOI is listed in the key resources table.
- Any additional information required to reanalyze the data reported in this paper is available from the lead contact upon request.

#### **EXPERIMENTAL MODELS AND SUBJECT DETAILS**

#### **Cell lines and culture conditions**

Most cell lines were obtained originally from primary vendors, then immediately expanded and frozen in multiple aliquots. Cell lines were validated based on known morphology, growth rates, and ferroptosis sensitivity. Low passage cells (<30 passages) were used



for all experiments. HT-1080 cells (sex: male) were obtained from ATCC (Cat# CCL-121, Manassas, VA). The polyclonal nuclear localized mKate2-expressing HT-1080 (HT-1080<sup>N</sup>), A375<sup>N</sup> (sex: male), H1299<sup>N</sup> (sex: male), T98G<sup>N</sup> (sex: male), H23<sup>Cas9,N</sup> (sex: male), and U-2 OSN (sex: female) cell lines were described previously (Conlon et al., 2021; Forcina et al., 2017; Inde et al., 2021; Tarangelo et al., 2018). PaTu 8988T (sex: female) and MIA PaCa2 (sex: male) cells were the kind gift of Rushika Perera (UCSF). HT-1080, HT-1080<sup>N</sup>, A375<sup>N</sup>, H1299<sup>N</sup>, T98G<sup>N</sup>, PaTu 8988T and MIA PaCa2 cells were cultured in Dulbecco's Modified Eagle Medium (DMEM, Cat# MT-10-013-CV, Thermo Fisher Scientific). U-2 OS<sup>N</sup> cells were cultured in McCoy's 5A medium (Cat# MT10050CV, Thermo Fisher Scientific). H23<sup>Cas9,N</sup> cells were cultured in RPMI 1640 medium (Cat# SH30027FS, Thermo Fisher Scientific). All growth media were supplemented with 10% fetal bovine serum (FBS, Cat# 26140-079, Gibco) and 0.5 U/mL Pen/Strep (P/S, Cat# 15070-063, Gibco). HT-1080 medium was additionally supplemented with 1x non-essential amino acids (NEAAs, Cat# 11140-050, Gibco). During routine passaging and cell seeding prior to experiments, cells were trypsinized and counted with a Cellometer Auto T4 cell counter (Nexelcom). Trypsin (Cat# 25200072) was from Gibco and PBS (Cat# 97062-338) from VWR.

GS187 gliomasoheres (sex: female) were derived from a sample isolated from a 59-year-old, newly diagnosed patient with no previous drug treatment through the UCLA Institutional Review Board (IRB) protocol 10-000655. The patient presented at clinic with headaches and neurologic complaints, MRI revealed masses in right temporal lobe and hippocampus, mass effect resulting in right uncal hemiation and 6 mm leftward shift of the septum pellucidum. The health and immune status of the patient is unknown. As previously described (Mai et al., 2017), gliomaspheres were cultured in DMEM/F-12 (Cat# 10-092-CV, Corning) supplemented with 1x B-27 supplement (Cat# 12587010, Thermo Fisher), 1x P/S, 1x GlutaMax (Cat# 35050-061, Life Technologies), heparin (5 μg/mL, Cat# H3149, Sigma), EGF (50 ng/mL, Cat# PHG0313, Fisher), and FGF-b (20 ng/mL, Cat# PHG0263, Fisher) added to the medium every 5 days and/or upon passaging. Gliomaspheres were passaged every 4-7 days into fresh media at 75,000-100,000 cells/mL following collection, centrifugation, and dissociation with TrypLE (Cat# 12605028, Thermo). One gliomasphere cell line was used for all experiments and individual cells from that cell line were randomly allocated to control or treatment groups. As is standard in cell biology, experiments were performed three times on separate days. All cell lines were grown at 37°C with 5% CO<sub>2</sub> in humidified tissue culture incubators (Thermo Scientific).

#### **METHOD DETAILS**

#### **Chemicals**

The structure of erastin2 (compound 35MEW28) was described (Dixon et al., 2014) and was synthesized by Acme (Palo Alto, CA). ML162 and CIL56 were synthesized by Acme. SYTOX Green (Cat# S7020) was from Life Technologies. INK128 (Cat# S2811), vinblastine (Cat# S1248), palbociclib (Cat# S1116), and nutlin-3 (Cat# S1061) were from Selleck Chemicals. Bovine serum albumin (BSA, Cat# 700-100P) was from Gemini Bio-Products or Sigma Aldrich (Cat# A3294). Torin 1 (Cat# 10997) was from Cayman Chemical. Rapamycin (Cat# BP2963-1), bortezomib (Cat# NC0587961), camptothecin (Cat# AC276721000) and Q-VD-OPh (Cat# OPH00101M) were from Fisher Scientific. BSO (Cat# AC23552-0010) was from Thermo Fisher Scientific. Staurosporine (Cat# S6942), ferrostatin-1 (Cat# SML0583), chloroquine (Cat# C6628), pepstatin A (Cat# P5318), leupeptin (Cat# L9783), and E-64 (Cat# E3132) were from Sigma-Aldrich. Ovalbumin (Cat# O-2577) was from A.G. Scientific. Casein (Cat# 218680) was from EMD Millipore. DQ-BSA was from Invitrogen (Cat# D12050). Deferoxamine mesylate (DFO, Cat# 14595) was from Cayman Chemical. FIN56 was a gift from Rachid Skouta, and CA074-Me and R11-OEt were kind gifts from Matthew Bogyo. C11 BODIPY 581/591 was dissolved in anhydrous methanol and all other chemical stocks were dissolved in DMSO except chloroquine, leupeptin, and E-64, which were dissolved in H2O, and BSO, which was dissolved directly into media. All chemicals were stored at -20°C until use. DFO was warmed at 37°C immediately before use.

#### Amino acid deprivation and protein supplementation media

To make cystine-free DMEM, 200 μM L-methionine and 4 mM L-glutamine were added to methionine, glutamine, and cystine-free DMEM (Cat# 17-204-CL, Corning, or Cat# 21013024, Thermo Fisher Scientific), to generate '-cystine DMEM'. This medium was supplemented with 10% dialyzed fetal bovine serum (dFBS, Cat# 26400044, Thermo Fisher Scientific) and 0.5 U/mL P/S. For experiments using HT-1080 cells, 1x NEAAs were added. For most albumin supplementation experiments, BSA was added to DMEM or -cystine DMEM at a concentration of 3% w/v (unless otherwise indicated) and sterile filtered. Ovalbumin and casein were added to DMEM or -cystine DMEM in the same manner as BSA. For leucine starvation experiments, cells were plated in DMEM for 24 h. The following day DMEM was removed and cells were rinsed twice with PBS. Cells were then cultured in serum-free RPMI 1640 medium (US Biological life science, Cat# R8999-03A) deficient for leucine. Chemical inhibitors were added along with changing DMEM medium to serum-free and leucine-free RPMI 1640 medium. Two h later, leucine (50 mg/mL), 5% double-dialyzed BSA (Sigma Aldrich, Cat# A3294), or 3% double-dialyzed bovine γ-globulin (Fisher scientific, Cat# ICN19147805) were added for 4 h.

#### **Cell death and proliferation tracking**

Cell death was assessed at multiple time points using scalable time-lapse analysis of cell death kinetics (STACK) (Forcina et al., 2017). 5,000 HT-1080<sup>N</sup> cells/well were plated the day before the experiment into 96-well plates (Cat# 07-200-588, Corning; or Cat# 07-200-91, Thermo). For 24 h pre-treatments, 2,500 cells/well were seeded instead. For cell panel experiments, cells were seeded in their native medium. The next day, the media in each well was removed and replaced with 200 µL of media for the experiment, all containing SYTOX green (20 nM). For cell panel experiments, all cells were treated with DMEM-based media. For experiments involving amino acid deprivation, cells were first washed once with HBSS (Cat# 14025134, Gibco) or PBS. Counts of live

#### **Article**



(mKate2 positive, mKate2<sup>+</sup>) and dead (SYTOX Green positive, SG<sup>+</sup>) cells were then counted every 2, 4, or 24 h using an Essen Incucyte Zoom Live-Cell Analysis System. SG<sup>+</sup> counts are always presented as the maximum observed at any given timepoint during the experiment. For cell proliferation data, only mKate2<sup>+</sup> counts were used. The following image extraction parameter values were used to count all cell lines except PaTu 8988T: for SG<sup>+</sup> objects: Adaptive threshold adjustment 10; Edge split on; Edge sensitivity -5; Filter area min 0  $\mu$ m<sup>2</sup>, max 750  $\mu$ m<sup>2</sup>; Eccentricity max 0.9; for mKate2<sup>+</sup> objects (in Nuc::mKate2 expressing cells): Adaptive threshold adjustment 1.0; Edge split on; Edge sensitivity 50; Filter area min 20  $\mu$ m<sup>2</sup>, maximum 8,100  $\mu$ m<sup>2</sup>; Eccentricity max 1.0; and for Overlap objects: Filter area min 20  $\mu$ m<sup>2</sup>, maximum 5,000  $\mu$ m<sup>2</sup>. For PaTu 8988T cells and their derivatives, SG<sup>+</sup> objects were counted using these parameters: Adaptive threshold adjustment 3.0; Edge split on; Edge sensitivity 0; Filter area min 15  $\mu$ m<sup>2</sup>, max 500  $\mu$ m<sup>2</sup>.

#### Glutathione quantification via Ellman's reagent

The day before samples were collected, 200,000 HT-1080 $^{\rm N}$  or PaTu 8988T cells were seeded into 6-well plates (Cat# 07-200-83, Corning). The next day, cells were washed with HBSS or PBS and treated in the conditions shown. Where applicable, HT-1080 $^{\rm N}$  cells were imaged in an Incucyte to determine cell number in each well. Then, cells were harvested on ice by scraping. Samples were then prepared for assessment of total intracellular glutathione (GSH+GSSG) using a glutathione quantification assay kit based on Ellman's reagent according mostly to the manufacturer's instructions (Cat# 703002, Cayman Chemical). To concentrate samples, cells were harvested into 250  $\mu$ L MES buffer instead of 500  $\mu$ L and the rest of the protocol was scaled down accordingly. When normalizing to protein content, a 30  $\mu$ L aliquot was taken before deproteination to assess protein levels using the BCA assay and the volumes for the rest of the assay were adjusted accordingly. Glutathione concentrations were calculated using a glutathione standard curve and normalized to cell count (HT-1080 $^{\rm N}$ ) or protein content (PaTu 8988T) in each sample.

#### Glutathione quantification via mass spectrometry

The day before the experiment, 200,000 PaTu 8988T NTC or CTSB<sup>KO</sup> cells were seeded into each well of 6-well plates. The next day, cells were washed once with PBS and treated in duplicate with 1 mL of the designated media and left for 24 h. After treatment, cells were washed on ice once in 1.5 mL/well with ice-cold 0.9% NaCl. For one duplicate, the saline was then removed, and the plates were moved to dry ice. 1 mL 80% methanol with internal standards was added to each well, cells were scraped thoroughly, and the solutions transferred to pre-chilled 1.5 mL microcentrifuge tubes. These tubes were then vortexed for 10 min at  $4^{\circ}$ C. Meanwhile, the other duplicates were harvested for BCA quantification for normalization as detailed above for western blotting. After vortexing, tubes were spun at  $18,200 \times g$  for 10 min at  $4^{\circ}$ C, and the supernatant transferred to new, pre-chilled microcentrifuge tubes and stored at  $-80^{\circ}$ C until quantification via mass spectrometry as described (Abu-Remaileh et al., 2017).

#### C11 BODIPY 581/591 imaging

For imaging on the confocal microscope, the day before the experiment, 100,000 cells/well were seeded into 6-well plates onto 22 mm #1.5 coverslips. The next day, the medium was removed, and cells were washed once with HBSS and treated with the given media. After 10 h, the treatment media were removed, and cells were washed once with HBSS. Then, C11 BODIPY 581/591 (5  $\mu$ M, Thermo Fisher Scientific, Cat# D3861) and Hoechst 33258 (1  $\mu$ g/mL, Thermo Fisher Scientific, Cat# H3569) were dissolved in HBSS and 1 mL was added to each sample. Cells were incubated at 37°C for 10 min. After 10 min, the labeling mixture was aspirated off and replaced with 1 mL fresh HBSS. The coverslip was removed from each well and inverted onto a glass microscope slide with 25  $\mu$ L of fresh HBSS. Imaging was performed using a Zeiss Axio Observer microscope with a confocal spinning-disk head (Yokogawa), PlanApoChromat 63x/1.4 NA oil immersion objective, and a Cascade II:512 electron-multiplying (EM) CCD camera (Photometrics). Imaging was performed on 3 independent biological replicates per treatment. Images were processed in ImageJ 2.0.0.

Other C11 imaging was conducted using a Lionheart FX automated microscope (BioTek). First, 7,500 (HT-1080) or 10,000 (PaTu 8988T) cells were seeded into each well of 96-well plates and treated the following day with designated conditions and labeled with C11 and Hoechst as described above but with PBS instead of HBSS. After labeling, fresh 1x PBS was applied to the cells. Then, the plate was immediately transferred to the Lionheart FX instrument. The plate was placed on a 37°C humidified stage, covered, and imaged in an automated mode with the following specifications: 20x, NA: 0.45 air objective; 3 × 3 montage at the center of each well; image acquisition using DAPI (filter cube 1225100/LED cube 1225000), GFP (12251010/1225001) and Texas Red (1225102/1225002). Images were analyzed using Gen5 v3.10 (BioTek).

#### **DQ-BSA** imaging

For live imaging on the Lionheart FX instrument, the day before the experiment,  $70,000\,\text{HT}-1080^N$  cells/well were seeded into 12-well plates. The next day, cells were pre-treated with DMSO, chloroquine, or protease inhibitors in HT-1080 medium for 1 h. Then, the media were changed to include  $0.1\,\text{mg/mL}$  DQ-BSA with the same inhibitors or vehicle and incubated at  $37^\circ\text{C}$  for 2 h. Next, media were changed to fresh media, still with the same inhibitors or vehicle for 1 h. Finally, the plate was imaged with the Lionheart FX instrument as for C11 imaging above, but with the following specifications:  $40x\,\text{Plan}$  Fluorite, NA: 50.6;  $2\times2$  montage in at least two separate locations per well; image acquisition using GFP (DQ-BSA) and Texas Red (nuclei). Raw (stitched) .tif files were then imported to ImageJ and analyzed with a macro available upon request.

For fixed-cell imaging, cells were seeded on glass coverslips in complete DMEM for 24 h. Cells were then starved of leucine for 2 h in serum-free DMEM in the presence of vehicle or indicated inhibitor. Cells were then incubated in serum-free medium supplemented with 0.5 mg/mL TMR-Dextran (Invitrogen, Cat# D12050) or 0.1 mg/mL DQ-BSA for 4 h. Subsequently, cells were washed 3 times with PBS



and fixed with 4% formaldehyde for 15 min. After fixation, cells were washed 3 times with PBS and mounted using a mounting medium with DAPI. When LysoTracker Red dye was used, 50 nM LysoTracker Red (Invitrogen, Cat# L7528) was added 1 h prior to fixation. Images were acquired on a Zeiss AxioVert200M microscope with a 63X oil immersion objective. The MetaMorph software package (Molecular Devices) was used to control the hardware and image acquisition. The excitation lasers used to capture the images were 488 nm and 561 nm. Images were processed with FIJI. Fluorescently labeled dextran or albumin was quantified using the mean fluorescence intensity determined by calculating the integrated signal from randomly chosen fields and normalized to the cell area.

#### **Western blotting**

For most western blots, the day before the experiment, 30,000 (72 h treatment) - 200,000 cells/well were seeded into 6-well plates (Cat# 07-200-83, Costar). The next day, if applicable, cells were treated as shown. For ATF4 time-course blots, 50,000 (48 h +cys, 10 h treatments), 100,000 (24 h), and 200,000 (48 h -cys treatments) cells were seeded and then treated to harvest all together. After treatment, the media were removed, and cells were washed twice on ice with 2 mL cold 1x PBS. Next, 40 µL cold RIPA + 0.1% SDS buffer with 5 mM NaF (Cat# S6776, Sigma-Aldrich) and 1:200 protease inhibitor cocktail P8340 (Cat# P8340, Sigma-Aldrich) was added and cells were scraped to harvest. Lysates were transferred to a 1.5 mL microcentrifuge tube and left on ice for 1 h to ensure full lysis, then stored at -80°C until needed or sonicated [1 s on, 1 s off, 60% amplitude) x 10 cycles, Fisher Scientific Model 120 Sonic Dismembrator (Thermo Fisher)] and spun down at 4°C (18,200 x g, 20 min). Cleared lysates were transferred to a new 1.5 mL tube and quantified using a BCA protein assay (Cat# 23252, Thermo Fisher Scientific) with a BSA standard curve. Equal amounts of protein were combined with 4x Bolt LDS Sample Buffer (Cat# B0007) and 10x Bolt Sample Reducing Agent (Cat# B0009) (Life Technologies), heated to 70°C for 10 min and run on a Bolt 4-12% Bis-Tris Plus Gel (Cat# NW04120BOX, Life Technologies). Protein was then transferred to a nitrocellulose membrane using an iBlot2 transfer stack (Cat# IB23001/2, Life Technologies), which was then blocked for 1 h at room temperature using Odyssey Blocking Buffer (Cat# 927-50000, LI-COR Biotechnology) or Intercept Blocking Buffer (Cat# 927-70001, LI-COR Biotechnology), and incubated in primary antibody mixture overnight at 4°C. Primary antibodies used were α-tubulin (Cat# MS581P1, Fisher Scientific, 1:10,000 dilution or, rarely, 1:2,000 dilution), α-TFRC (Cat# 13-6800, Thermo Fisher Scientific, 1:10,000 dilution) entific, 1:1000), α-β-Actin (Santa Cruz Biotechnology, Cat# sc-47778, 1:1000), α-p53 (Santa Cruz Biotechnology, Cat# sc-126, 1:200), α-Rb (BD Biosciences, Cat# 554136, 1:1000), α-Raptor (Millipore Sigma, Cat# 09-21709-217), α-FSP1 (Cat# 20886-1-AP, Proteintech), α-GPX4 (Cat# ab125066, Abcam), α-CTSL (Cat# ab200738, Abcam), α-phospho-S6K1 (Cat# 9234), α-S6K1 (Cat# 2708), α-phospho-RPS6 (Cat# 4858S, 1:1000), α-RPS6 (Cat# 2217S, 1:1000), α-phospho-4E-BP1 (Thr 37/46, Cat# 2855T, 1:1000), α-4E-BP1 (Cat# 9644S, 1:1000), α-phospho-Rb (Cat# 8516S, 1:250), α-phospho-Akt (Cat# 4056S, 1:1000), α-Akt (Cat# 9272S, 1:1000), α-ULK1 (Cat# 6439), α-CTSB (Cat# 31718S, 1:1000), α-CTSD (Cat# 2284), α-ATF-4 (Cat# 11815S, 1:1000), α-IRP2 (Cat# 37135S, 1:1000), α-ATG7 (Cat# 2631S, 1:1000), α-GAPDH (Cat# 2118S, 1:1000), or α-LC3B (Cat# 2775S, 1:1000) (Cell Signaling Technologies). The membrane was washed 3x for seven min each in TBST and then incubated in secondary antibody mixture (55 min, room temperature, 1:1 TBST and Odyssey or Intercept blocking buffer). Secondary antibodies used were donkey α-rabbit (Cat# 926-68023/32213, LI-COR Biotechnology, 1:15,000 dilution) and donkey α-mouse (Cat# 926-68022/926-32212, LI-COR Biotechnology, 1:15,000 dilution). The membrane was then washed 3x for seven min each in TBST and scanned on an Odyssey CLx Imaging System (LI-COR). Western blots were performed on three independent biological replicates unless otherwise indicated. Western blots in Figures 4B, S5C, and S5D were conducted as follows. The day before the experiment, 400,000-500,000 PaTu 8988T or 1,000,000-1,200,000 MIA PaCa2 cells were seeded into each well of 6-well plates. The next day, cells were starved and treated as described. Cell lysates were prepared in ice-cold lysis buffer (40 mM HEPES pH 7.4,1% Triton X-100, 10 mM β-glycerol phosphate, 10 mM pyrophosphate, 2.5 mM MgCl2 with Complete EDTA-free Protease Inhibitor Cocktail (Roche) and Phosphatase Inhibitor Cocktail (Roche)). The soluble fractions from lysates were collected by centrifugation at 17,000 x g for 10 min in a cold centrifuge. Lysates were then quantified using a BCA protein assay and equal amounts of protein were resolved by 8-16% SDS-PAGE at 120 V. Resolved proteins were transferred for 2 h at 45 V to ethanol-pretreated PVDF membranes to be further analyzed by immunoblotting. Membranes were blocked with 5% nonfat dry milk prepared in TBST (Tris-buffered saline with Tween 20) for 1 h, then incubated overnight with primary antibodies in 5% bovine serum albumin (BSA) in TBST at 4°C. All primary antibodies were used at (1:500-1:1000) dilution. Following incubation, membranes were washed 3x for 5 min each with TBST and then incubated with the appropriate secondary antibodies diluted 1:3000 in 5% milk for 1 h at room temperature. Membranes were then washed three

#### Virus generation and use

To generate lentiviruses bearing shRNAs, plasmids encoding scramble, RPTOR, or RICTOR shRNAs (which were gifts from David Sabatini, Addgene plasmids #1864, #1858, and #1853, respectively) were co-transfected with 3<sup>rd</sup> generation lentiviral packaging plasmids (pMDLg/pRRE and pRSV-Rev, which were gifts from Didier Trono, Addgene plasmids #12251 and #12253 respectively, and pCMV-VSV-G, which was a gift from Bob Weinberg, Addgene plasmid #8454) into HEK293T cells using PolyJet (SignaGen Laboratories, Cat# SL100688) as per manufacturer instructions. Viral supernatant was harvested 48 and 72 h later, combined, filtered through a 0.45 µm PVDF filter (EMD Millipore, Cat# SLHV033RS), and stored in single-use aliquots at -80°C until use. For CTSB, CTSD, CTSL and ATG7 disruption, lentiviruses were produced by co-transfecting HEK-293T cells with pLentiCRISPRv1 (with sgRNA cloned) alongside the packaging plasmids VSV-G envelope and  $\Delta$ VPR. The following sense (S) and antisense (AS) oligo-nucleotides were cloned into pLentiCRISPRv1 (see Table S1 for oligonucleotide sequences). For adding back CTSB expression, retroviruses were produced by co-transfecting HEK-293T cells with pMXs-CTSB plasmid and retroviral packaging plasmids Gag-Pol and

times with TBST before being visualized using ECL western blotting substrate.





VSV-G using XtremeGene9 transfection reagent. The culture medium was changed to DMEM supplemented with 30% inactivated fetal calf serum 16 h post transfection. The virus-containing supernatant was collected 48 h post transfection and spun for 5 min at 400 x g to remove cells and then frozen at  $-80^{\circ}$ C. For re-introducing CTSB, cells were seeded at a density of 2 ×  $10^{6}$  cells/mL in DMEM containing 8  $\mu$ g/mL polybrene (EMD Millipore), and then transduced with retrovirus by centrifugation at 2,200 RPM for 45 min at 37°C. After a 16-18 h incubation, cells were re-seeded into fresh medium containing blasticidin (InvivoGen, Cat# ant-bl-10p) and selected for 72 h. Stable cell lines were confirmed by the expression of CTSB by western blot.

#### mTORC1 and mTORC2 shRNA-mediated gene silencing

Knockdowns were performed as described (Conlon et al., 2021). Briefly, HT-1080 (immunoblot) or HT-1080<sup>N</sup> (viability) cells were seeded in either 6-well plates (immunoblot, at 30,000 cells/well) or 96-well plates (viability, at 1,000 cells/well). The next day, medium was removed and replaced with HT-1080 medium with 8  $\mu$ g/mL polybrene (Sigma-Aldrich, Cat# H9268) and vehicle control or viral supernatant at an MOI of  $\sim$ 3. 48 h later, the media were removed and replaced with HT-1080 medium containing 2  $\mu$ g/mL puromycin (Life Technologies, Cat# A11138-03). The un-transduced wells were instead treated with 1  $\mu$ M INK128. 24 h later, cells in 6-well plates were harvested for immunoblots as described above, and cells in 96-well plates were washed and treated as described above for viability experiments.

#### **CRISPR/Cas9** genome editing

HT-1080 CTNS gene disrupted cell lines were generated with the sgRNA sequence GCCAGCCTACCCGGTCTGAT. First, two oligos (see Table S1) were annealed at a concentration of 10 μM at 37°C for 30 min, followed by 95°C for 5 min, and cooled to 25°C at a rate of 5°C per min. The oligo duplex was then ligated into the plasmid pSD224 and transformed into DH5α. Plasmid DNA was extracted with a QIAGEN spin column (Cat# 27106, QIAGEN) and validated by DNA sequencing. For transfection, 150,000 HT-1080 cells were seeded into each of two wells of a 6-well plate. The next day, 1 µg plasmid (or water for mock) was mixed with 2 µL lipofectamine LTX (Life Technologies Cat# 15338-100), incubated for 15 min, and added dropwise onto cells. The next day, transfection medium was removed and replaced with fresh medium. After a 24 h recovery, GFP+ cells were single cell-sorted using a BD FACSJazz Cell Sorter (BD Biosciences) (Stanford Shared FACS Facility) into a 96-well plate containing DMEM + 30% FBS, 1x NEAAs and 0.5 U/mL P/S. Cells were incubated at 37°C until they grew into colonies. Individual colonies were expanded. DNA was harvested using the NucleoSpin Tissue kit (Clontech, Cat# 740952.250) according to manufacturer instructions and sent for sequencing. KO clones were confirmed to have homozygous frameshift mutations at the sgRNA site. For transduction to disrupt CTSB, CTSD, CTSL and ATG7, cells were seeded at a density of 1.5  $\times$  10<sup>6</sup> cells/mL in DMEM containing 8  $\mu$ g/mL polybrene (EMD Millipore), and then transduced with lentivirus by centrifugation at 2,200 RPM for 45 min at 37°C. Cells were incubated for 16-18 h, then selected with puromycin for 72 h. After transduction, cells were single-cell FACS-sorted into 96-well plates. Knockout clones were identified by immunoblotting. Note that for ATG7 gene-disrupted cell lines that KO1 was isolated from cells trandusced with the first guide RNA (KO1), while KO2 and KO3 were independently isolated from cells transduced with the second guide RNA (KO2). Control cells were generated by targeting the AAVS1 locus as described (Wang et al., 2015).

#### Spheroid cell culture and experiments

Cells to make spheroids were seeded in  $100~\mu L$  at 10,000~cells/well in 96-well ultra-low adhesion plates (PerkinElmer, Cat #6055330) and left to establish for 72~h. Daily progress was monitored using an Incucyte. Then,  $100~\mu L$  containing 2x treatment concentrations was carefully added to each well to start the experiment. Daily images were taken with an Incucyte. For spheroid western blots, multiple wells were prepared for each condition, and 20,000-30,000~cells were seeded in parallel in wells of 6-well plates to generate monolayer lysates. 72~h later, cells were treated  $\pm~1~\mu M$  INK128. 24~h later, cells in monolayer were trypsinized, quenched, transferred to 15~mL conical tubes, and put on ice. Spheroids were collected by pipetting media including spheroids, pooling wells by condition, and transferring to 15~mL conical tubes. Cells were pelleted by centrifuge at 1000~x~g, then washed with 10~mL ice-cold PBS, pelleted, washed again, then pelleted again. PBS was removed and 20- $100~\mu L$  RIPA buffer with NaF and P8340 was added to each sample. Samples were then immediately sonicated, cleared, and subsequently processed as detailed above. Spheroid viability was ascertained using the CellTiter-Glo assay (Cat# G7572, Promega) according to manufacturer instructions.  $100~\mu L$  medium was removed from each well and replaced with the mixed CellTiter-Glo assay reagent. Luminescence was counted using a Cytation3 plate reader (BioTek Instruments), background-subtracted using empty wells, and normalized to the DMSO control for each condition.

#### **QUANTIFICATION AND STATISTICAL ANALYSIS**

Lethal fraction calculations were performed using Microsoft Excel (Microsoft Corporation, Redmond, WA) as described (Forcina et al., 2017) with one modification to account for red/green double positive objects, i.e. dead cells still transiently expressing detectable nuclear mKate2 signal (Inde et al., 2021): the lethal fraction at a given time was calculated as: 1 - ((mKate2+ - (mKate2+G+))/(SG+ + (mKate2+G+)))). Densitometry on western blots was performed using ImageJ. Lionheart FX image analysis was performed using ImageJ or Gen5 v3.10 software (BioTek). Serum proteome abundance data (Geyer et al., 2016) and cysteine percent calculations were performed in RStudio, version 1.4.1106 running R version R-4.0.5. R code available upon request. Plotting was performed using GraphPad Prism 8.4/9.0 (GraphPad Software, La Jolla, CA). Figures were assembled using Adobe Illustrator 25.3.1 (Adobe Systems, San Jose, CA).